Bol 8. Escala de distancias extragaláctica

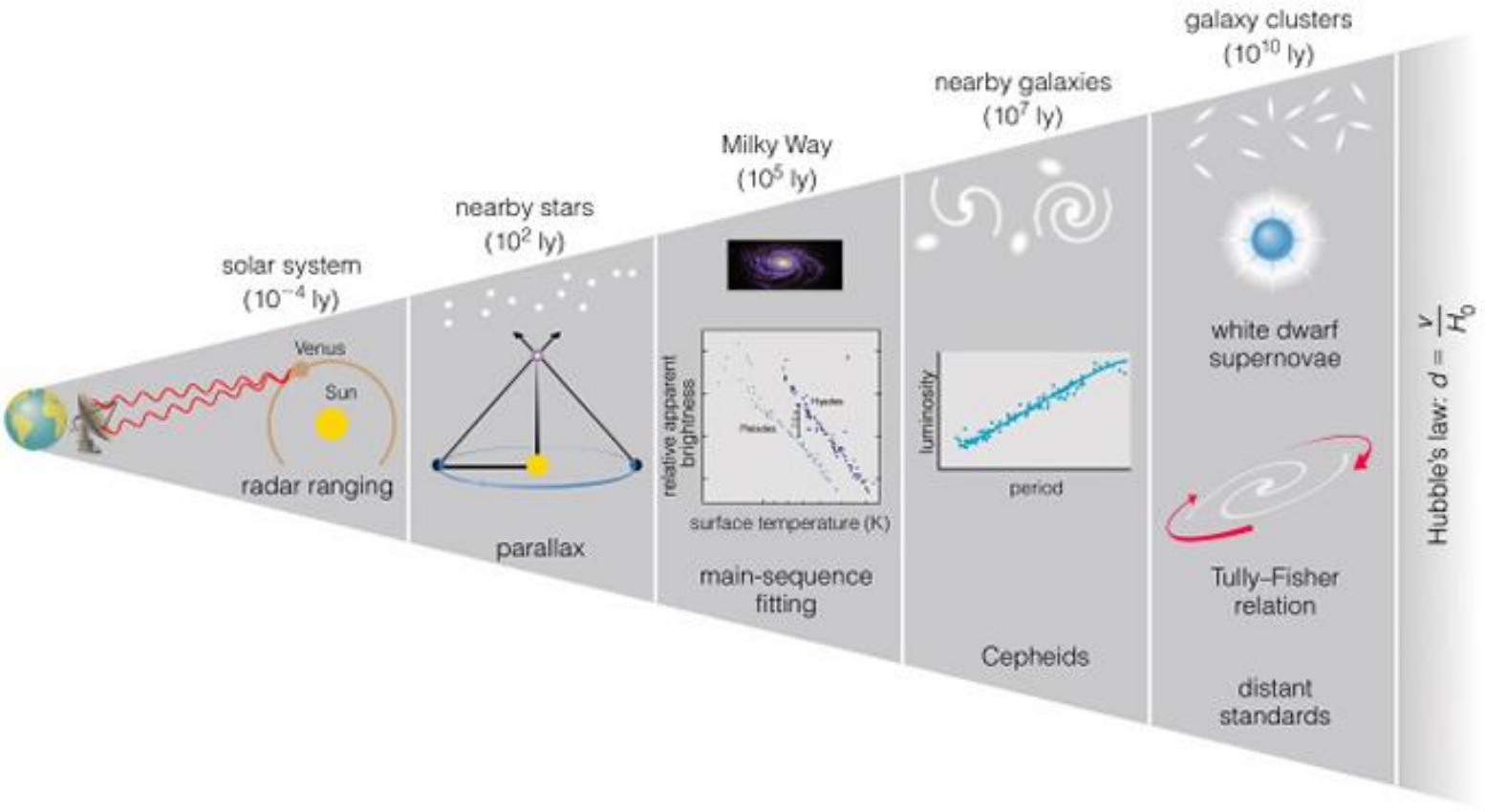

Indicadores primarios y secundarios

La determinación de distancias en la *escala de nuestra galaxia* se basa en paralajes trigonométricas, paralajes estadísticas, cúmulos en movimiento, ajuste de la ZAMS, etc. Para medir mayores distancias, fuera de la Vía Láctea, es necesario recurrir a otros indicadores que suelen agruparse en dos categorías: indicadores primarios y secundarios. Según distintos autores, se incluyen en cada una a indicadores diferentes. En nuestro caso, no se pretende establecer una clasificación definitiva, y seguiremos la propuesta de Czerny et al. (2018):

"The formal division of the distance indicators into primary and secondary leads to difficulties in description of methods which can actually be used in two ways: with, and without the support of the other methods for scaling."

Así, consideraremos *indicadores primarios* aquellos que no requieren utilizar otros métodos para su uso, y *secundarios* aquellos que necesitan recurrir a opciones intermedias (por ej. indicadores primarios, modelos, hipótesis, etc) para su aplicación. Veremos ejemplos de cada categoría.

[*Nota:* la obtención de la distancia *generalmente* surge, en el paso final, de comparar mag absoluta y mag aparente en igual banda (módulo de distancia), o por geometría relacionando medida angular y medida lineal de un dado objeto o una dada característica.]

Indicadores Primarios:

P1- Cefeidas clásicas
P2- RR Lyr
P3- Cefeidas tipo II
P4- Novas (poco uso)

Indicadores Secundarios:

S1- Extremo de la rama de gig rojas (TRGB)
S2- Relación de Tully-Fisher (gal S)
S3- Relación de Faber-Jackson (gal E)
S4- Supernovas tipo Ia (SNIa)
S5- Supernovas tipo II (SNII)
S6- Función de luminosidad de Nebulosas planetarias
S7- Función de luminosidad de Cúmulos globulares
S8- Ley de Hubble-Lemaître

P1- *The Cepheid variable distance scale*

The observational basis of this distance scale was provided by Henrietta Leavitt whilst working at the Harvard College Observatory where she became head of the photographic photometry department. In the early years of the twentieth century, her group studied images of stars to determine their magnitude using a photographic measurement system developed by Leavitt that covered a 17 magnitude brightness range. Many of the plates measured by Leavitt were taken at Harvard Observatory's southern station in Arequipa, Peru from which the Magellanic Clouds could be observed and she spent much time searching the plates taken there for variable stars within them. She discovered many variable stars within them including 25 Cepheid variable stars. These stars are amongst some of the brightest; between 1000 and 10 000 times that of our Sun and are named after the star Delta Cephei which was discovered to be variable by the British astronomer John Goodricke in 1784. These stars pulsate regularly rising rapidly to peak brightness and falling more slowly, as shown in Figure 8.21a. Leavitt determined the periods of 25 Cepheid variables in the SMC and in 1912 announced what has since become known as the famous period–luminosity relationship (Figure 8.21b). She stated: 'A straight line can be readily drawn among each of the two series of points corresponding to maxima and minima (of the brightness

of Cepheid variables), thus showing that there is a simple relation between the brightness of the variable and their periods.' As the SMC was at some considerable distance from Earth and was relatively small, Leavitt also realized that: 'as the variables are probably nearly the same distance from the Earth, their periods are apparently associated with their actual emission of light, as determined by their mass, density, and surface brightness.'

The relationship between a Cepheid variable's luminosity and period is quite precise, and a 3-day period Cepheid corresponds to a luminosity of about 800 times the Sun whilst a 30-day period Cepheid is 10 000 times as bright as the Sun.

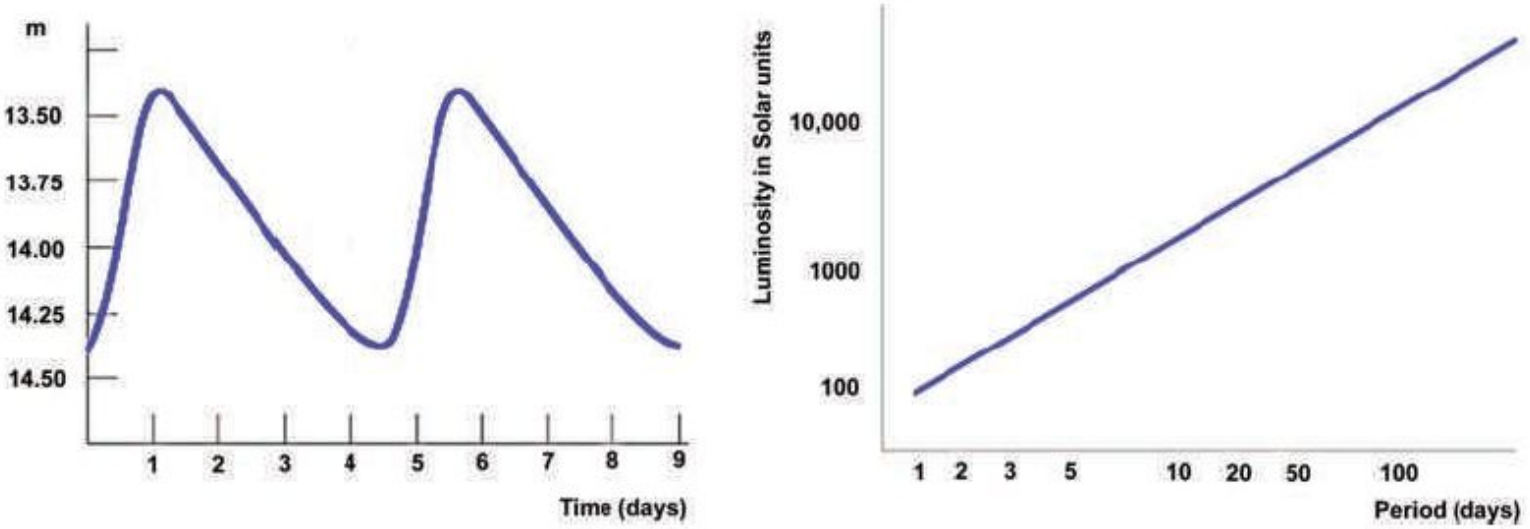

Figure 8.21 (a) A Cepheid variable light curve and (b) the period–luminosity relationship.

P1- Relación P- L de Cefeidas clásicas (o CefeidasTipo I):

“Leavitt Law”

$$mag = \alpha + \beta \log P$$

► *para cada filtro*

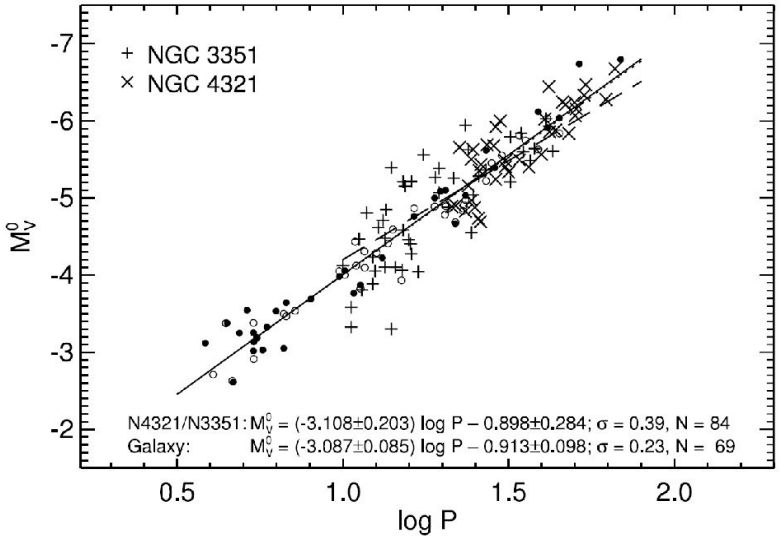

FIG. 2.—*P-L* relation in *V* of metal-rich Cepheids in the Galaxy (*circles*), NGC 4321 (*crosses*), and NGC 3351 (*plus signs*). The latter two galaxies define a slope in good agreement with the Galaxy (*dotted line*). For comparison the LMC *P-L* relation for log $P > 1.0$ is shown as a dashed line.

Tammann et al. 2008, ApJ 679, 52

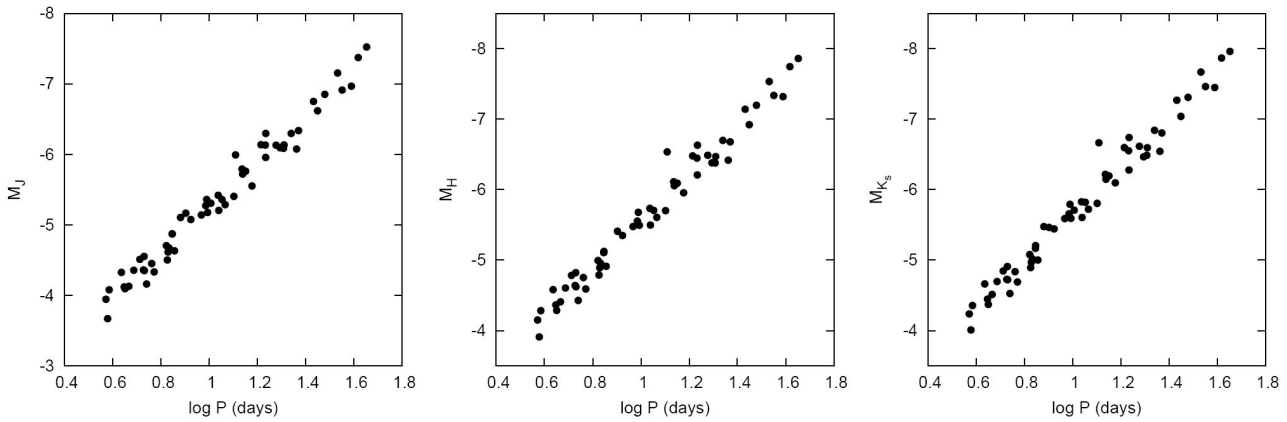

Fig. 3. Adopted Galactic *PL* relations in near-infrared bands.

Fouqué et al. 2007, A&A 476, 73

Relación P- L de Cefeidas clásicas

Ventajas

- instrínsecamente **brillantes** (Mv ~-2 a -7)
- abundantes en galaxias S
- fáciles de identificar por su curva de luz
- siguen relación P-L de baja dispersión (con coef diferentes según el filtro, es una rel. P-L-color)
- tiempo de vida largo, se pueden re-observar
- variabilidad bien estudiada (modelos, etc)
- mejores *calibraciones* con **paralajes trigon.** y estadísticas con Hipparcos. Más recientemente, con **Cefeidas de la Vía Láctea y de las Nubes de Magallanes con GAIA.**

Desventajas

- dependencia de la rel. P-L con la **metalicidad**
- al ser jóvenes están en zonas con polvo (**absorción y enrojecimiento**)
- se pueden medir en galaxias S **hasta d~30Mpc** con HST

[*Distancia a la LMC*: con *binarias eclipsantes "detached"* (separadas), de P largos (60-700d) y estrellas tardías, se obtienen radios lineales y con interferometría en NIR los radios angulares.]

Relación P- L de Cefeidas clásicas

Efecto de la metalicidad en Cefeidas Galácticas y de las Nubes de Magallanes:

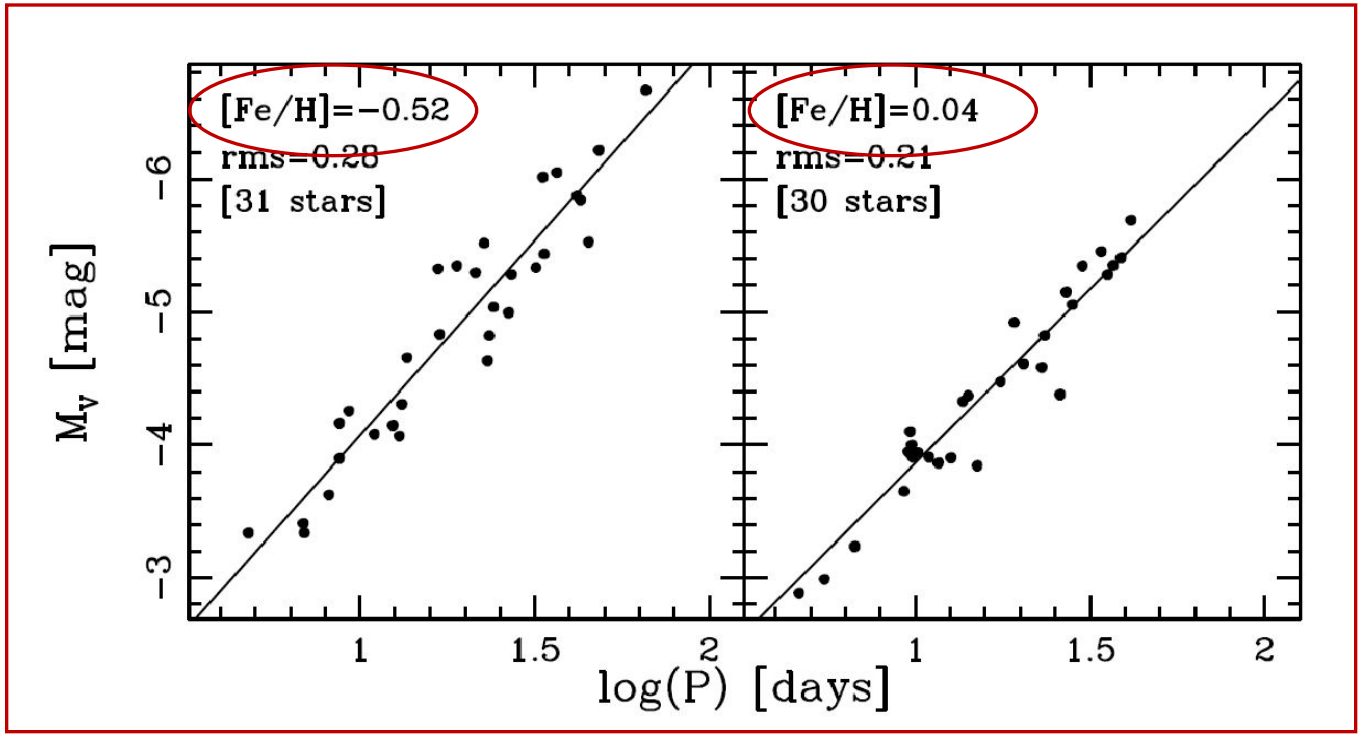

Romaniello et al. 2008,
A&A 488, 731

Relación P-L de Cefeidas clásicas en la LMC (Nube Mayor de Mag.)

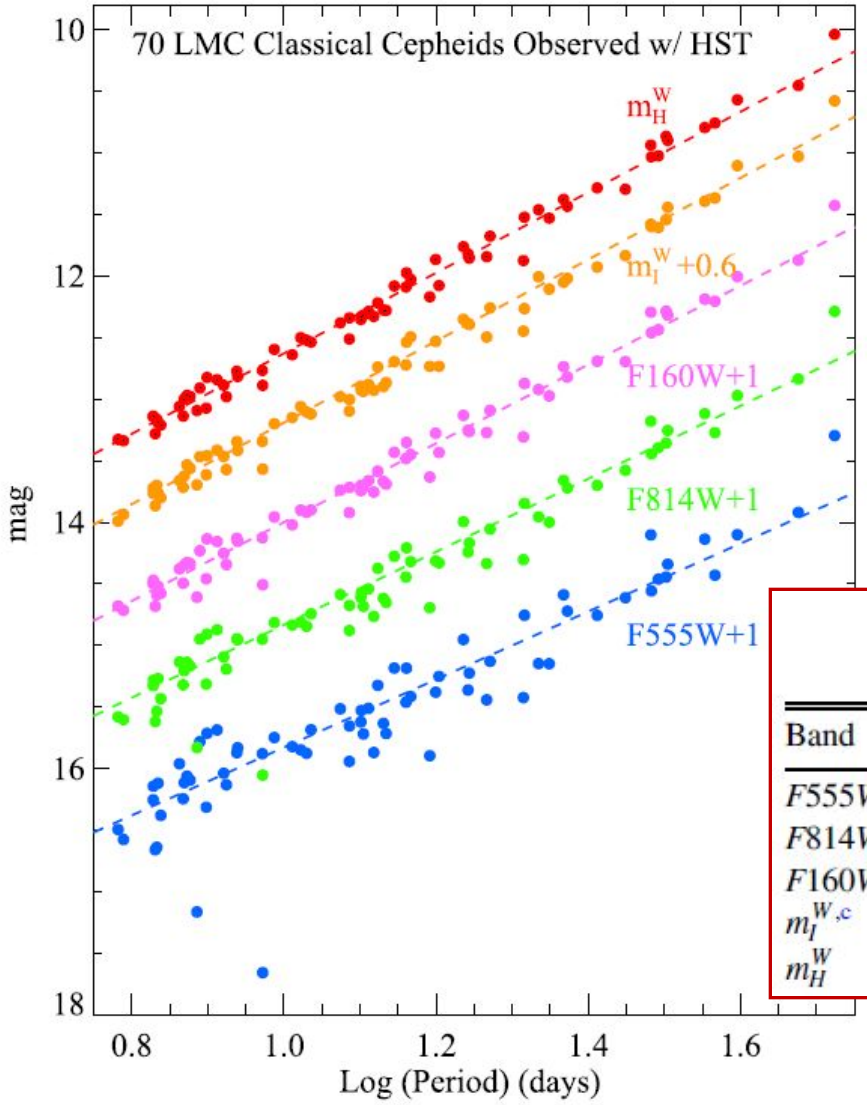

Figure 3. Period–mean magnitude relation for the 70 LMC Cepheids with slopes and statistics given in Table 3.

Filtros HST: F555W (**V**)
F814W (**I**)
F160W (**H**)

Table 3
Period–Mean magnitude Relations from *HST* LMC Cepheids

Band	Slope[a]	Intercept[b]	Scatter[b]
F555W	−2.76	17.638	0.312
F814W	−2.96	16.854	0.202
F160W	−3.20	16.209	0.104
$m_I^{W,c}$	−3.31	15.935	0.085
m_H^W	−3.26	15.898[d]	0.075

Wesenheit indices, $m_H^W = m_{F160W} - 0.386(m_{F555W} - m_{F814W})$
and $m_I^W = m_{F814W} - 1.3(m_{F555W} - m_{F814W})$.

Riess et al. 2019,
ApJ 876, #85

P2- Magnitudes absolutas V de RR Lyrae

a) *RR Lyrae and HB stars. Trigonometric Parallaxes*

$$M_V(RR) = 0.18([\mathrm{Fe/H}] + 1.5) + 0.62 \pm 0.11.$$

el error del punto de cero es muy importante pues va a afectar directamente al error en distancia.

b) *RR Lyrae and HB stars. Statistical Parallaxes*

$$M_V(RR) = 0.18([\mathrm{Fe/H}] + 1.5) + 0.73 \pm 0.12.$$

c) *RR Lyrae and HB stars. The Baade-Wesselink method.*

$$M_V(RR) = 0.18([\mathrm{Fe/H}] + 1.5) + 0.71 \pm 0.08.$$

ver slide 12

Carretta et al. 2000, ApJ 533, 215

Las RR Lyrae son estrellas evolucionadas (queman He en el núcleo), de baja masa y baja metalicidad. Típicas de Población II. Se encuentran en cúmulos globulares y también como estrellas de campo del halo y disco grueso de gal espirales, en gal elípticas e irregulares. Fáciles de encontrar (períodos: 0.2 a 1.2 días), con poco efecto de polvo. <Mv> ~ 0.75 +/- 0.1

 intrínsecamente más débiles que las Cefeidas clásicas, pero se llega hasta el Grupo Local. Dist **hasta 2-3 Mpc**.

Relación *período–metalicidad–luminosidad en IR* y relación *metalicidad – luminosidad en la banda V*, de RR Lyrae

- Dambis et al. 2013 (MNRAS 435, 3206)
  Mediante **paralajes estadísticas**, con ~400 RR Lyr de campo en la Vía Láctea.
  Mov propios, velocidades radiales, buena determinación de extinción interestelar, fotometría en visual e IR, y metalicidades.

En NIR, la relación período-metalicidad-luminosidad:

$$\langle M_{Ks} \rangle = -0.769 + 0.088\,[Fe/H] - 2.33 \log P$$

Y en el visual, la relación metalicidad-luminosidad:

$$\langle M_{V} \rangle = 1.094 + 0.232\,[Fe/H]$$

Método de Baade-Wesselink para estrellas pulsantes

Consider a pulsating star at minimum, with a measured temperature T_1 and observed flux f_1 with radius R_1, then:

$$f_1 = \frac{4\pi R_1^2 \sigma T_1^4}{4\pi D^2}$$

Similarly at maximum, with a measured temperature T_2 and observed flux f_2 with radius R_2:

$$f_2 = \frac{4\pi R_2^2 \sigma T_2^4}{4\pi D^2}$$

Note: T_1 , T_2 , f_1 , f_2 are directly observable. Just need the radius…
So, from spectroscopic observations we can get the photospheric velocity $v(t)$, from this we can determine the change in radius, ΔR:

$$R_2 = R_1 + \Delta R = R_1 + \int_{t_1}^{t_2} v(t)\, dt$$

➔ **3 equations, 3 unknowns, solve for R_1, R_2, and D**

Difficulties lie in modeling the effects of the stellar atmosphere, and deriving the true radial velocity from what we observe.

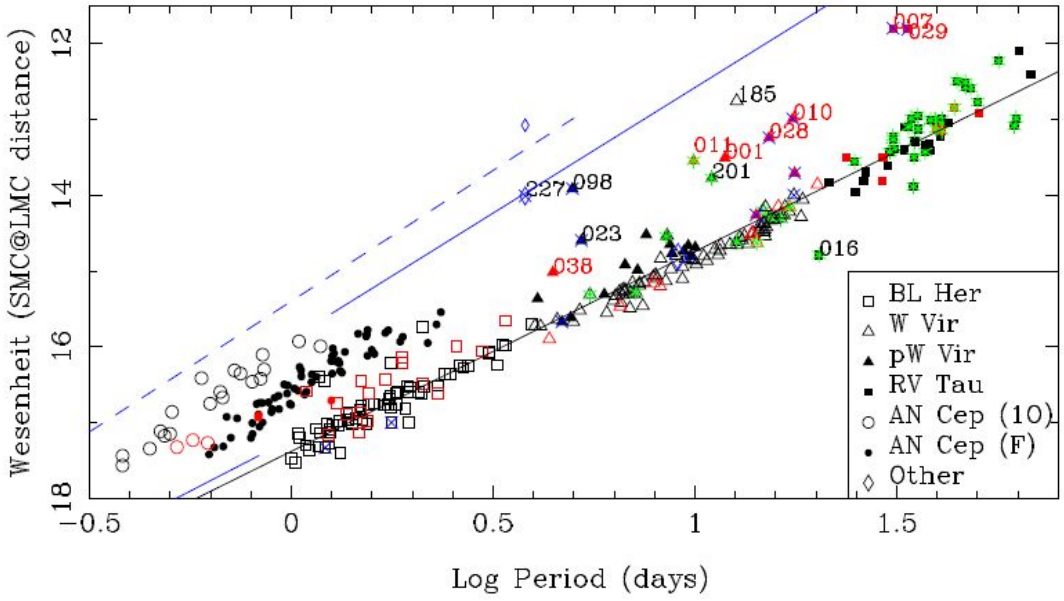

Fig. 1. Wesenheit PL relation. Stars in the SMC are plotted in red and shifted to the distance of the LMC. Some outliers are indicated with their identifier. Stars with an IR excess according to GJ17 are indicated by a green plus sign. Stars that show eclipsing or ellipsoidal variations according to OGLE are indicated by a blue cross. Stars plotted as a blue diamond are OGLE-LMC-CEP-0227 (the classical Cepheid in an eclipsing binary system, at $P = 3.79$ days) and the Galactic T2C κ Pav (at $P = 9.08$ days) scaled to the distance of the LMC (see text). For −0227 both the system value (the smaller, brighter point) and the Wesenheit magnitude of the Cepheid in the system (from Pilecki et al. 2013) are plotted. The black solid line shows the relation derived from the BLH + WVIR + non-dusty RVTs with periods below 50 days in the LMC (see Table 1), plotted over the entire period range. The blue lines indicate the Wesenheit relation for CC in the LMC from Soszyński et al. (2008a) for FU (solid line) and FU (dashed line) pulsators and the relation for RRab stars (at $\log P < -0.08$) from Soszynski et al. (2003).

P3- Relac P-L de Cefeidas Tipo II

1 < P < 4d: BL Herculis

4 < P < 20d: W Virginis

20 < P < 70d : RV Tauri

Son est. de Pob II, pobres en metales y de baja masa (~ 1 $M_{\odot}$). Presentes en las NM y cúmulos globulares (principalmente en el halo de la Vía Láctea). Trazan poblaciones estelares viejas.

Siguen una relación P-L pero son ***intrísecamente mucho más débiles*** que las Cefeidas Tipo I.
La *metalicidad* parece afectar de distinto modo a cada subgrupo.

Wesenheit magnitude W :

$$W = I - 1.55 \cdot (V - I)$$

Groenewegen & Jurkovic 2017
AA 604, A29

Comparaciones (esquema):

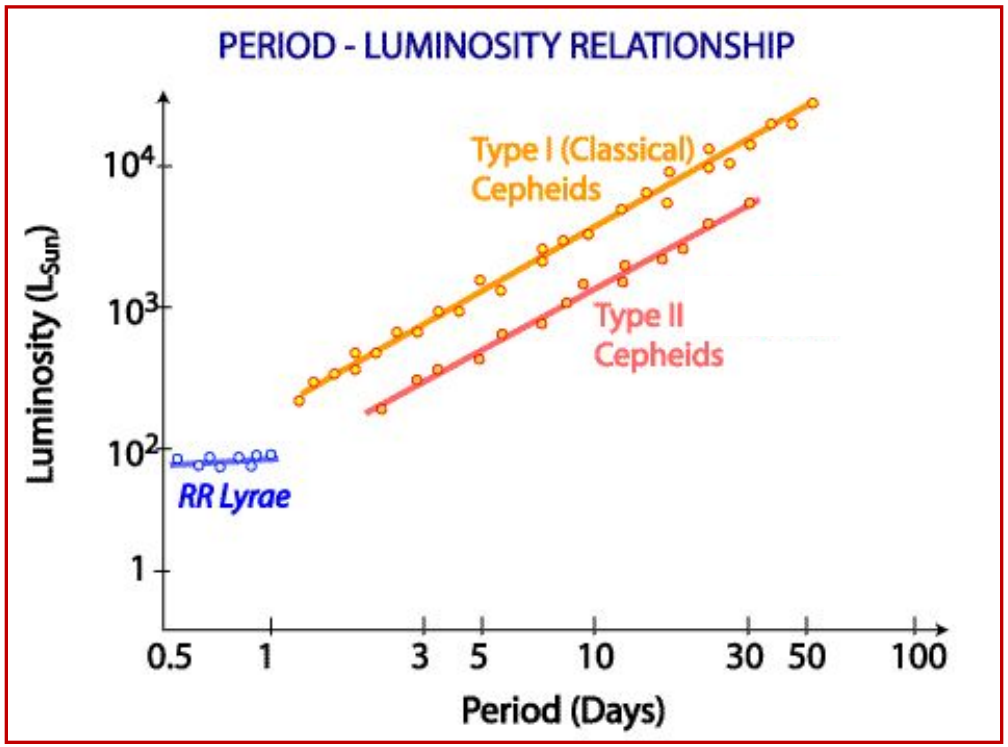

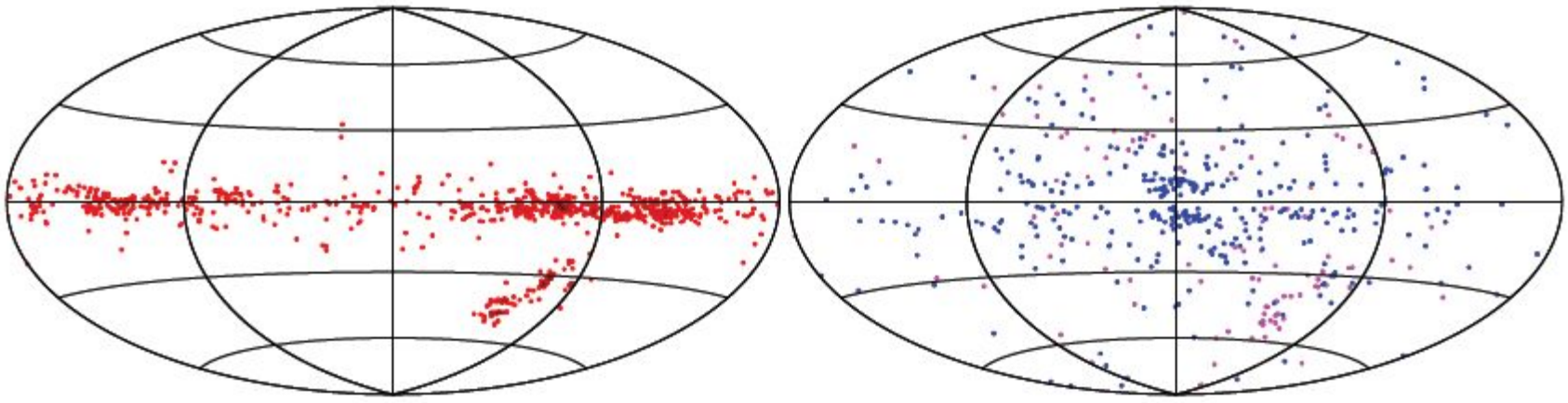

Proyección Aitoff en coordenadas Galácticas. Izq: Cefeidas Clásicas, Der: Cefeidas Tipo II

P4- Relación $M_{V\_máx}$ vs. velocidad de decaimiento del brillo en Novas

Novas: sistemas binarios cercanos en que una enana blanca recibe masa (rica en H) de su compañera menos evolucionada, que llena su lóbulo de Roche. Muestran un aumento de brillo rápido y repentino por reacciones termonucleares al caer ese material sobre la superficie de la enana blanca. Durante la explosión ("outburst") son más brillantes que las Cefeidas y se identifican a grandes d (**hasta 50 Mpc**).

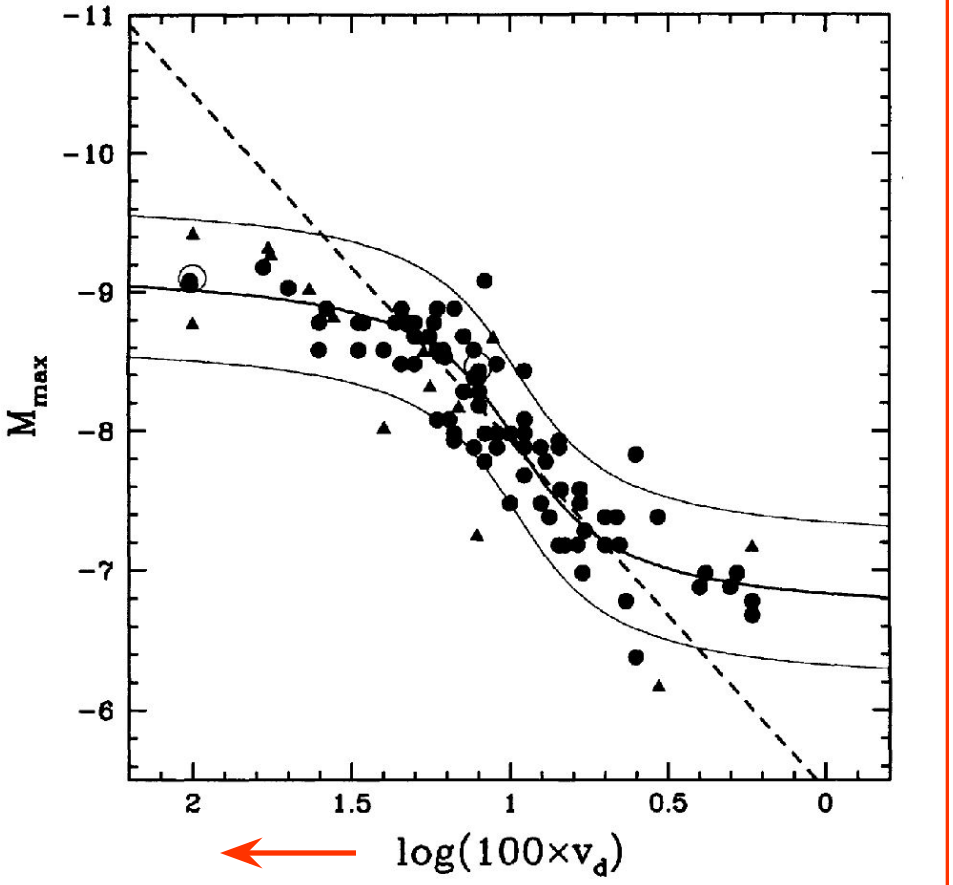

Mag en el máx puede llegar a $M_v \sim -10$.

Relación MMRD ("max mag rate decline"): entre mag en el máximo y la velocidad de decaimiento de la curva de luz.

$$M_{max} = A + B \log (2 / t_2)$$

$$\mathbf{v_d = 2 / t_2}$$

$\mathbf{t_2}$ [días]: tiempo en que el brillo de la nova decae 2 mag por debajo del máximo.

Della Valle & Livio 1995
ApJ 452, 704

Relación $M_{V\_máx}$ vs. velocidad de decaimiento del brillo en Novas

❖ Cómo se calibra?

- Con Novas de nuestra Galaxia, mediante técnicas geométricas (“paralajes de expansión” en que se mide el tamaño y velocidad de expansión de la cáscara o “shell”), funciona como *indicador primario.*
- Con novas de M31 (Andrómeda) y la LMC, por ejemplo, se utiliza la distancia a ellas determinada por otros métodos (Cefeidas, SNIa), y en este caso funciona como un *indicador secundario*.

Se ha llegado a observar novas no sólo en galaxias S sino en elípticas del cúmulo de Virgo.

❖ Desventajas

- No se puede predecir el momento de la explosión.
- Requiere observaciones muy cercanas al máximo.

Ambas condiciones llevan a que se necesite *mucho tiempo de telescopio*. Por ese motivo son *poco utilizadas*.

S1- Brillo del extremo de la rama de gigantes rojas (TRGB)

La referencia en este método es el *brillo en el extremo de la RGB*, que por ej en los DCMs de cúmulos globulares se observa que para los de menor contenido de metales se ubica en una magnitud aprox. constante.

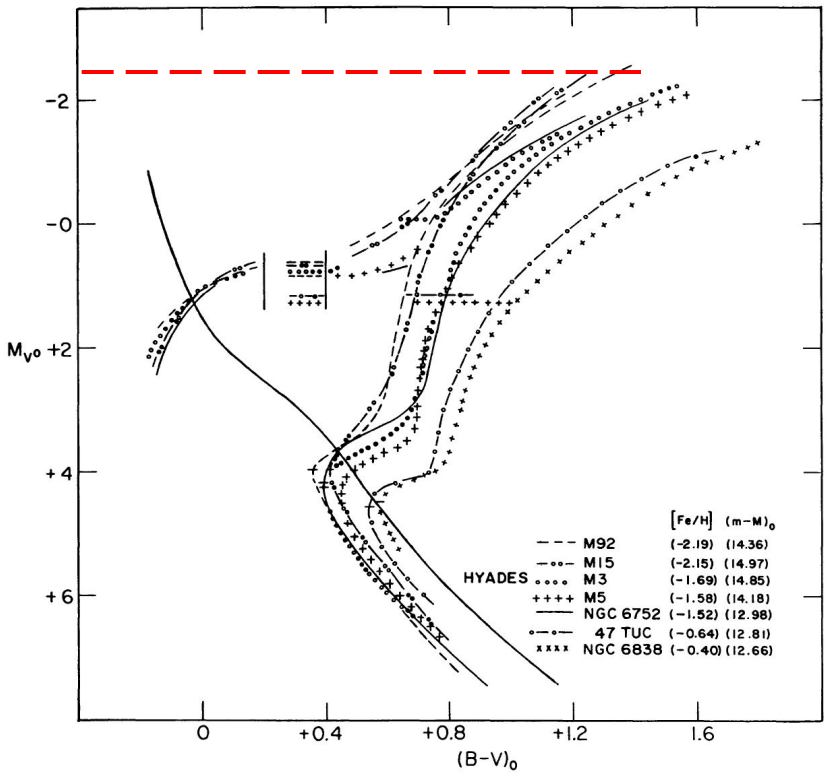

Fig. 2 The composite CMD for seven globular clusters. Note that the brightest red giant stars of the five most metal-poor clusters have very similar absolute magnitudes of about $M_V = -2.5$ (from Sandage 1986b). The I magnitude of the brightest red giants is even more stable near $M_I = -4.05$ as found by Da Costa & Armandroff (1990).

Tammann et al. 2008, A&ARv 15, 289

Para aplicar este método se requiere construir el DCM de la galaxia, para ubicar allí la posición del extremo de la RGB, que corresponde a estrellas en la etapa del *flash de He*.
Por lo tanto es necesario poder "resolver" las estrellas (observar las estrellas individualmente para que c/u de ellas represente un punto en el DCM).
Dados estos requerimientos, el método TRGB se puede aplicar a:

- galaxias que contengan estrellas de ~población II (estrellas viejas y pobres en metales) para que correspondan a una magnitud del TRGB ~cte. Las estrellas más brillantes en este tipo de poblaciones son gigantes rojas, que en general son abundantes.
  - esto es, edad > 7 Gyr y metalicidad -2.3 < [Fe/H] < -0.7
- galaxias enanas, halos de galaxias (poco efecto de polvo)
- se puede llegar a galaxias **hasta d ~ 20 Mpc** con el telescopio Hubble (~cúmulo de Virgo).

- valor de referencia: magnitud absoluta en banda I para el "tip" M_I (TRGB) = -4.05 ± 0.1

- Cómo se calibra?
- con cúmulos globulares de la Vía Láctea (con distancias determinadas con RR Lyr o paralajes de estrellas subenanas).
- con modelos, dado que el flash de He es un proceso bien comprendido.

Se aplica midiendo la mag aparente del TRGB del DCM de la galaxia en cuestión (o en la función de luminosidad) y, conocida la mag absoluta, se calcula el módulo de distancia.

DCM de la galaxia M32, ubicación del TRGB

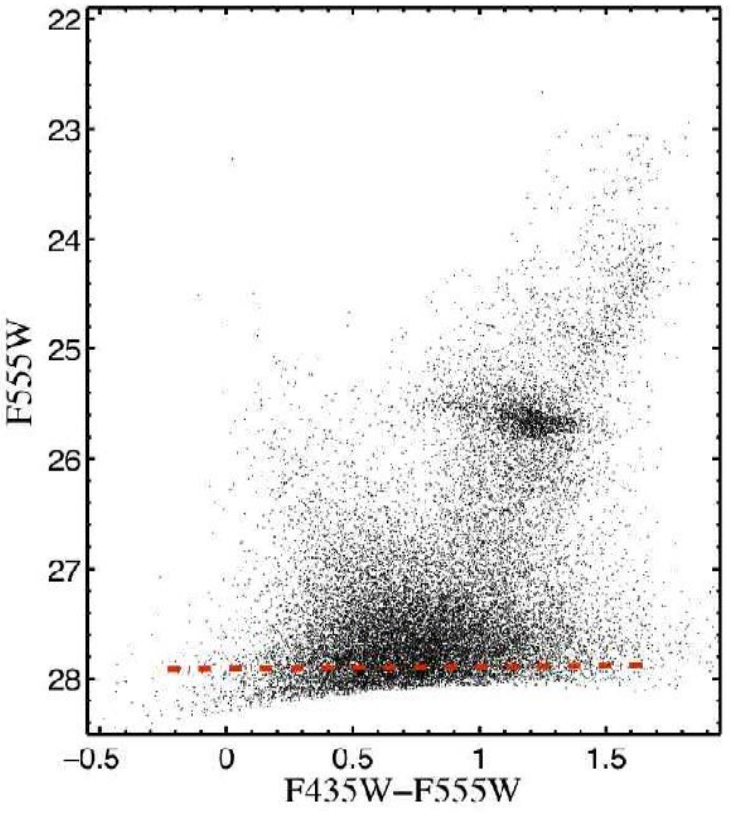

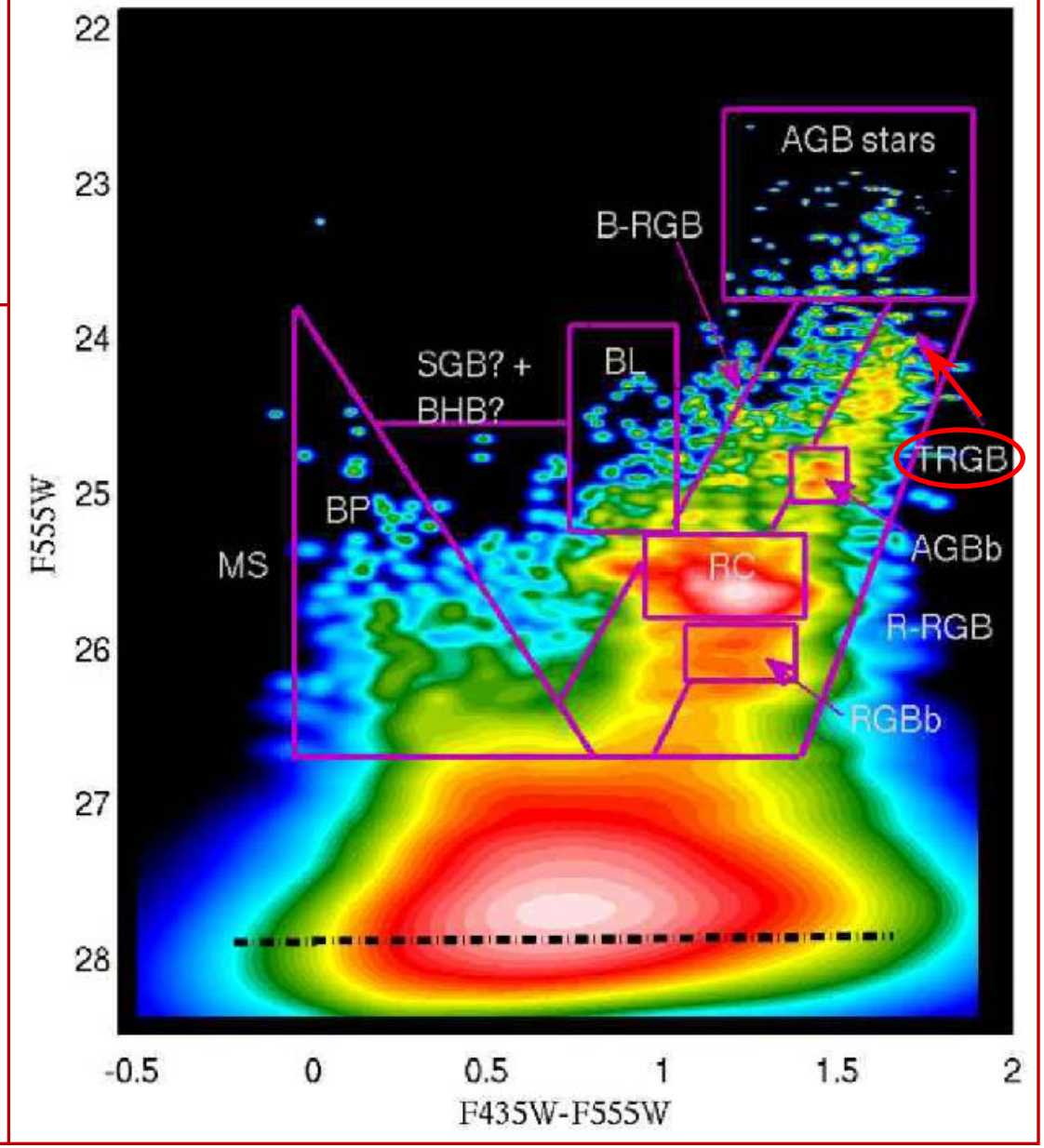

Monachesi et al. 2011, ApJ 727, 55

S2- The Tully–Fisher relation

Using 21 cm observations of spiral galaxies, in 1977 R. Brent Tully and J. Richard Fisher found that the maximum rotation velocity of spirals is closely related to their luminosity, following the relation

$$L \propto V_{\text{rot máx}}^4 \leftarrow L \propto v_{\max}^{\alpha}, \qquad (3.19)$$

where the power-law index (i.e., the slope) of the Tully–Fisher relation is about $\alpha \sim 4$. The larger the wavelength of the filter in which the luminosity is measured, the smaller the dispersion of the Tully–Fisher relation (see Fig. **(1)**). This is to be expected because radiation at larger wavelengths is less affected by dust absorption and by the current star formation rate, which may vary to some extent between individual spirals. Furthermore, it is found that the value of α increases with the wavelength of the filter: The Tully–Fisher relation is steeper in the red, which follows from the fact that more massive, or more luminous galaxies—i.e., those with larger $v_{\max}$—are redder, as can be seen from Fig. **(1)** The dispersion of galaxies around the relation (3.19) in the near-infrared (e.g., in the H-band) is about 10 %.

Because of this close correlation, the luminosity of spirals can be estimated quite precisely by measuring the rotational velocity. The determination of the (maximum) rotational velocity is independent of the galaxy's distance. By comparing the luminosity, as determined from the Tully–Fisher relation, with the measured flux, one can then estimate the distance of the galaxy—without utilizing the Hubble relation!

The measurement of $v_{\max}$ is obtained either from a spatially resolved rotation curve, by measuring $v_{\text{rot}}(\theta)$, which can be done with optical spectroscopy or, for relatively nearby galaxies, also with spatially resolved 21 cm spectroscopy. Alternatively, one can observe an integrated spectrum of the 21 cm line of HI that has a Doppler width corresponding to about $2v_{\max}$ (see Fig. 3.28). The Tully–Fisher relation shown in Fig. **(1)** was determined by measuring the width of the 21 cm line.

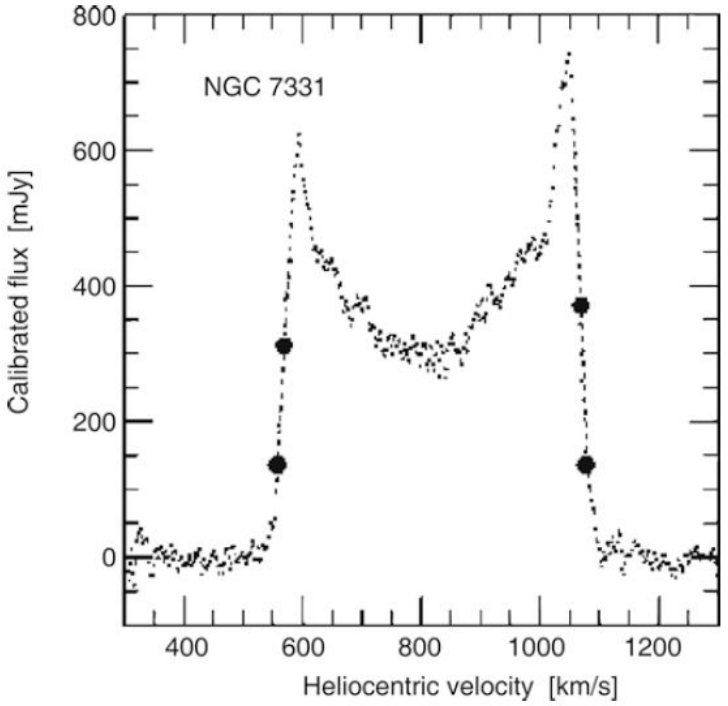

Fig. 3.28 21 cm profile of the galaxy NGC 7331. The *bold dots* indicate 20 and 50 % of the maximum flux; these are of relevance for the determination of the line width from which the rotational velocity is derived.

Relación de Tully - Fisher (TF)

Fig (1)

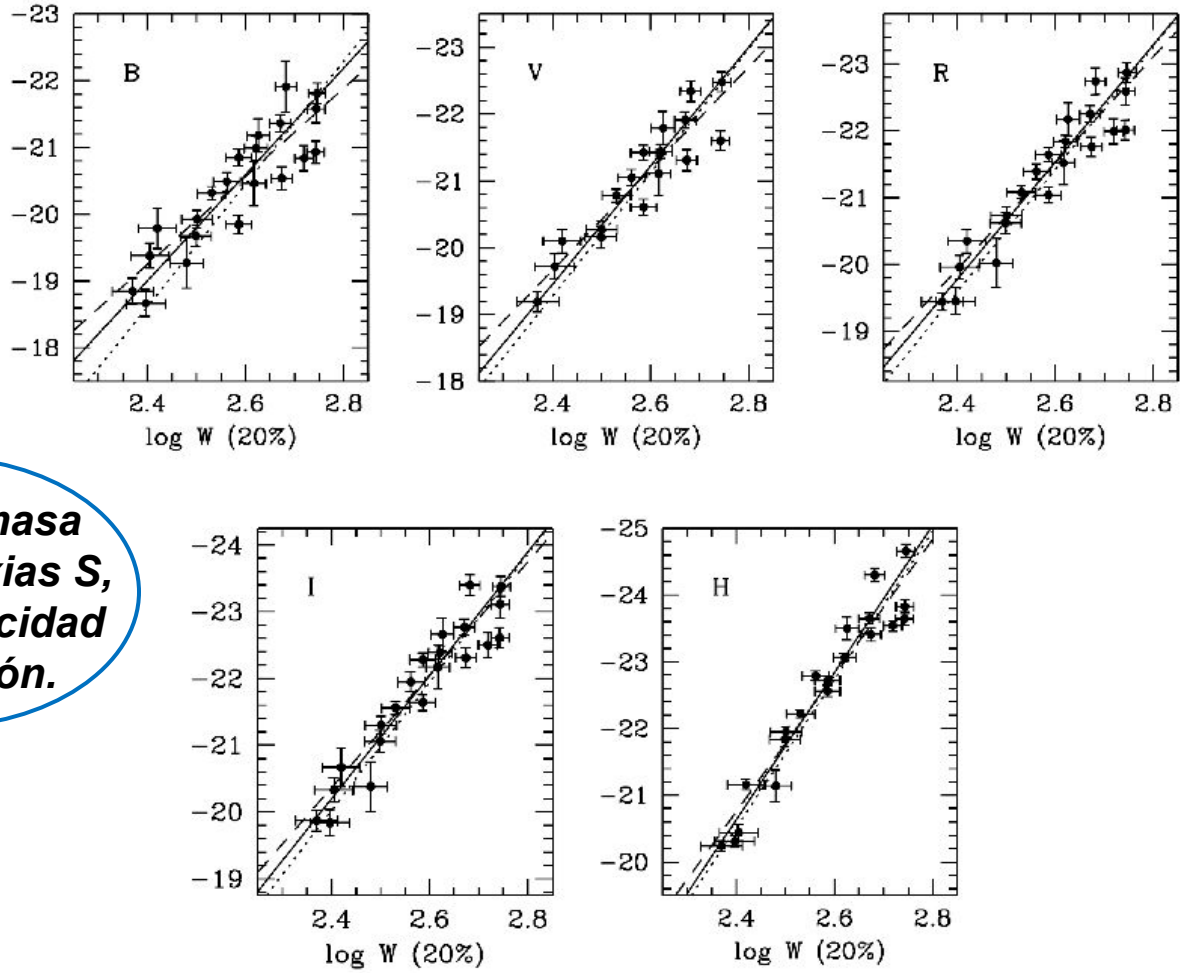

A mayor masa de las galaxias S, mayor velocidad de rotación.

FIG. 1.—$BVRIH_{-0.5}$ Tully-Fisher relations for spiral galaxies with Cepheid distances, using 20% line width. Solid lines represent the bivariate fits, while the dotted and dashed lines represent inverse and direct fits, respectively.

Sakai et al. 2000, ApJ 529, 698
HST Key Project

Relación de Tully - Fisher (TF)

- Cómo se aplica?

En *las galaxias S dominan los movimientos "organizados", esto es la rotación* en el disco. Se observa la galaxia espiral en radio y se mide el ancho de la línea de 21 cm . El ancho del perfil W se mide a un dado % del máximo, se corrige por turbulencia, por inclinación de la galaxia, por la forma del perfil, etc ($W \propto 2\, V_{\text{rot máx}}$). Con la relación de TF se obtiene la mag absoluta (en IR es más precisa), y luego con la magnitud aparente de la galaxia en la misma banda, se calcula el módulo de distancia.

- Cómo se calibra la relación de TF?

A partir de galaxias S de distancias conocidas por otros métodos, por ej. con Cefeidas.

- Con la relación de TF se puede determinar distancias de **hasta ~300 Mpc.**

The baryonic Tully–Fisher relation. The above 'derivation' of the Tully–Fisher relation is based on the assumption of a constant M/L value, where M is the total mass (i.e., including dark matter). Let us assume that (1) the ratio of baryons to dark matter is constant, and furthermore that (2) the stellar populations in spirals are similar, so that the ratio of stellar mass to luminosity is a constant. Even under these assumptions we would expect the Tully–Fisher relation to be valid only if the gas does not, or only marginally, contribute to the baryonic mass. However, low-mass spirals contain a significant fraction of gas, so we should expect that the Tully–Fisher relation does not apply to these galaxies. Indeed, it is found that spirals with a small $v_{\rm max} \lesssim 100\,{\rm km/s}$ deviate significantly from the Tully–Fisher relation—see Fig. **(2)** a.

Since the luminosity is approximately proportional to the stellar mass, $L \propto M_*$, the Tully–Fisher relation is a relation between $v_{\rm max}$ and M_*. Adding the mass of the gas, which can be determined from the strength of the 21 cm line and molecular emission, to the stellar mass, a much tighter correlation is obtained, see Fig. **(2)** b. It reads

$$M_{\rm disk} = 2\times 10^9\, h^{-2}\, M_\odot \left(\frac{v_{\rm max}}{100\,{\rm km/s}}\right)^4 , \qquad (3.24)$$

and is valid over five orders of magnitude in disk mass $M_{\rm disk} = M_* + M_{\rm gas}$. If no further baryons exist in spirals (such as, e.g., MACHOs), this close relation means that the ratio of baryons and dark matter in spirals is constant over a very wide mass range.

Relación de Tully - Fisher bariónica

$\mathcal{M}_\star$/L = cte (para c/tipo de gal)

- $\mathcal{M}_\star$

$\mathcal{M}_d = \mathcal{M}_\star + \mathcal{M}_{gas}$

Fig (2)

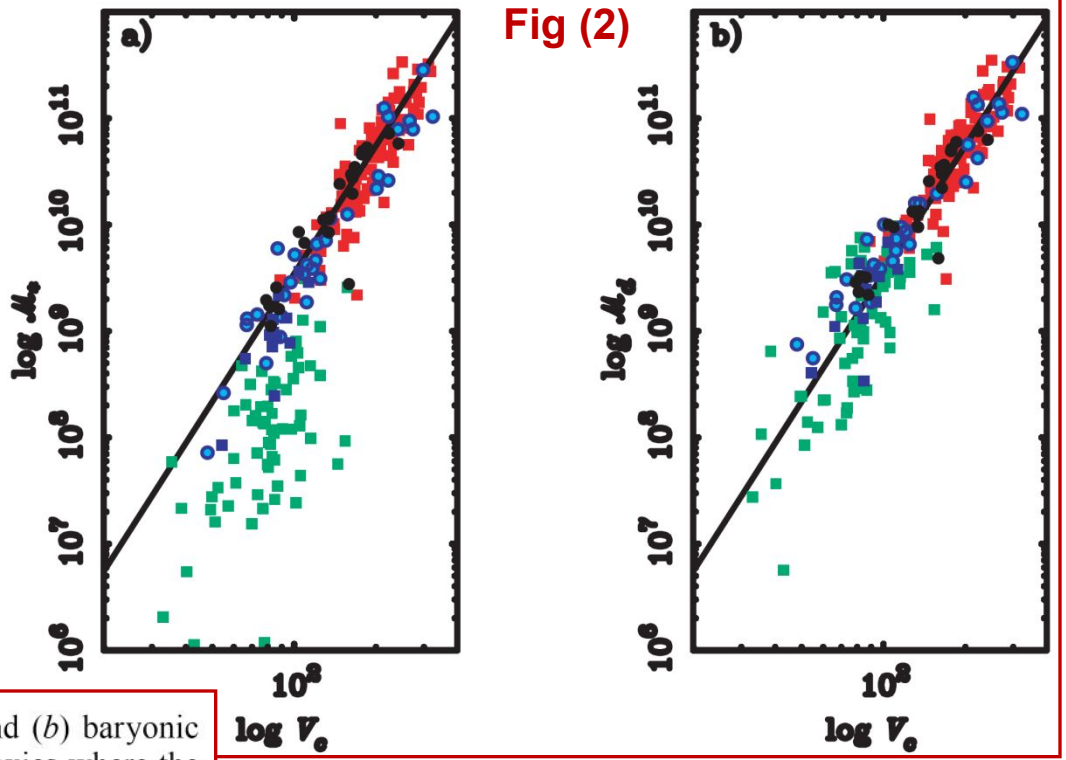

FIG. 1.—Tully-Fisher relation plotted as (*a*) stellar mass and (*b*) baryonic disk mass against rotation velocity. The squares represent galaxies where the circular velocity is estimated from the line width by $V_c = \frac{1}{2}W_{20}$, while the circles have $V_c = V_{\rm flat}$ from resolved rotation curves. The data employed include the *H*-band data of Bothun et al. (1985; *red*), the *K*′-band data of Verheijen (1997; *black*), and the *I*-band data of Pildis et al. (1997) with velocities as reported by Eder & Schombert (2000; *green*). Also shown are the *B*-band data of McGaugh & de Blok (1998; *light blue*) and of Matthews et al. (1998; *dark blue*). The stellar mass is computed from the luminosity by assuming a constant mass-to-light ratio ($M_* = \Upsilon_* L$), so (*a*) is directly analogous to the usual luminosity–line width diagram. We assume mass-to-light ratios for the stellar populations of late-type galaxies of $\Upsilon_*^B = 1.4$, $\Upsilon_*^I = 1.7$, $\Upsilon_*^H = 1.0$, and $\Upsilon_*^{K'} = 0.8\ M_\odot/L_\odot$ (see text). In (*b*), we plot the total baryonic disk mass $M_d = M_* + M_{\rm gas}$ with $M_{\rm gas} = 1.4 M_{\rm H\,I}$. In (*a*), a clear break is apparent. Galaxies with $V_c \lesssim 90$ km s^{-1} fall systematically below the Tully-Fisher relation defined by brighter galaxies. In (*b*), the deficit in mass apparent in (*a*) has been restored by including the gas mass. The solid line is an unweighted fit to the red-band data in (*b*) with a correlation coefficient of 0.92 and a slope indistinguishable from 4.

McGaugh et al. 2000, ApJ 533, L99

S3- Relación de Faber-Jackson (D_n – σ) / Plano fundamental de las galaxias elípticas

The Faber–Jackson relation

A relation for elliptical galaxies, analogous to the Tully–Fisher relation, was found by Sandra Faber and Roger Jackson. They discovered that the velocity dispersion in the center of ellipticals, σ_0, scales with luminosity (1976)

$$L \propto \sigma_0^4 \quad , \quad \text{or} \quad \log(\sigma_0) = -0.1 M_B + \text{const.}$$

A mayor masa de las galaxias E, mayor dispersión de veloc.

En la práctica se utiliza una relación entre el diámetro D_n de la isofota de brillo superficial promedio en el azul $<\mu_B>$= 20.75 mag/arcsec^2 y la dispersión central de veloc de la galaxia elíptica σ_0: $\log D_n$ vs. $\log \sigma_0$

- Cómo se aplica?

En las *galaxias E dominan los movimientos al azar*, por eso medimos la dispersión de veloc a partir de espectros (tomados ppalmente sobre la zona central, de mayor brillo) y con el ancho de las líneas se obtiene la dispersión σ_0 en [km/s]. Teniendo la dispersión, se calcula el diámetro **D_n [kpc]** con la relación de F-J , y con imágenes se mide el diámetro **D_n [arcsec]**. Con ambas medidas de D_n se calcula la distancia.

- Se requieren observaciones de imágenes y espectros.

❖ Cómo se calibra la relación de F-J?

No hay galaxias E brillantes suficientemente cercanas que puedan calibrarse por otros métodos, por lo tanto se consideran grupos o cúmulos de galaxias que contengan galaxias espirales, calibradas a su vez con Cefeidas, y se asume que todas las galaxias del grupo/cúmulo están a igual distancia. Por ej, se utilizan los cúmulos de Virgo o Fornax, grupo de Leo, etc.
[Se elige esa isofota particular porque es la que *minimiza* la dispersión de la relación F-J.]

El plano fundamental de las galaxias elípticas

Así como las relaciones TF y F-J establecen una relación entre la luminosidad y propiedades cinemáticas de galaxias S y E, respectivamente, en el caso de las galaxias E existe otra relación entre parámetros observables que *tiene menor dispersión que la relación F-J.* Es el *plano fundamental* (Djorgovski & Davis 1987, ApJ, 313, 59), que es una representación de la dinámica de las Es y establece una relación entre brillo superficial efectivo promedio (esto es dentro de la isofota de radio r_e y en unidades de intensidad), tamaño (radio efectivo) y temperatura cinética (o sea dispersión de velocidades):

$$\log r_e = A \cdot \log \langle I_e \rangle + B \cdot \log \sigma$$

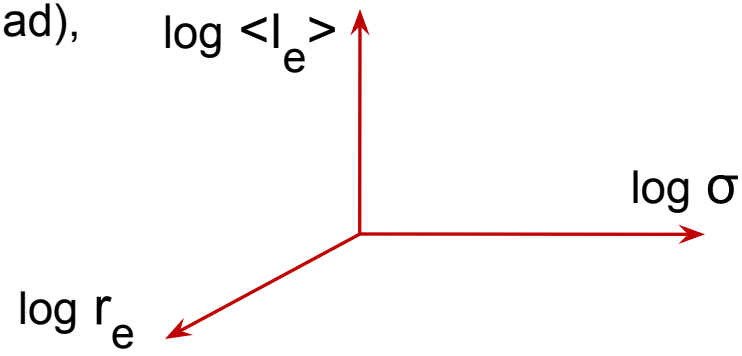

Asi, las galaxias E se ubican sobre un plano de baja dispersión en ese espacio de 3D. La relación de F-J es una proyección en 2D de este plano.
[Recordemos que el radio efectivo es el que contiene la mitad de la luz de la galaxia.]

Mould (2020): "*The fundamental plane of early type galaxies is fairly aptly named, because in the 3-space of velocity dispersion, surface brightness and effective radius is expressed the dynamical equilibrium that a galaxy has reached… It has long been understood that the virial theorem will place quiescent galaxies with a well-defined mass to light ratio in a plane in this space*."

❖ Cómo se aplica?

Al igual que en el método de F-J, medimos la dispersión de velocidades a partir de espectros y se requiere además obtener el brillo sup efectivo promedio de imágenes. Con ellos, se calcula el radio efectivo $\mathbf{r_e}$ **[kpc]** aplicando la relación del plano fundamental, y de las imágenes se mide el radio efectivo en medida angular $\mathbf{r_e}$ **[arcsec]**.

Con ambas medidas de r_e se calcula la distancia.

❖ Cómo se calibra el plano fundamental?

Al igual que en el método de F-J, se consideran grupos o cúmulos de galaxias que contengan galaxias espirales, calibradas a su vez con Cefeidas, y se asume que todas las galaxias del grupo/cúmulo están a igual distancia. Por ej, se utilizan los cúmulos de Virgo o Fornax, grupo de Leo, etc.

Plano fundamental y relación D_n - σ (Faber - Jackson)

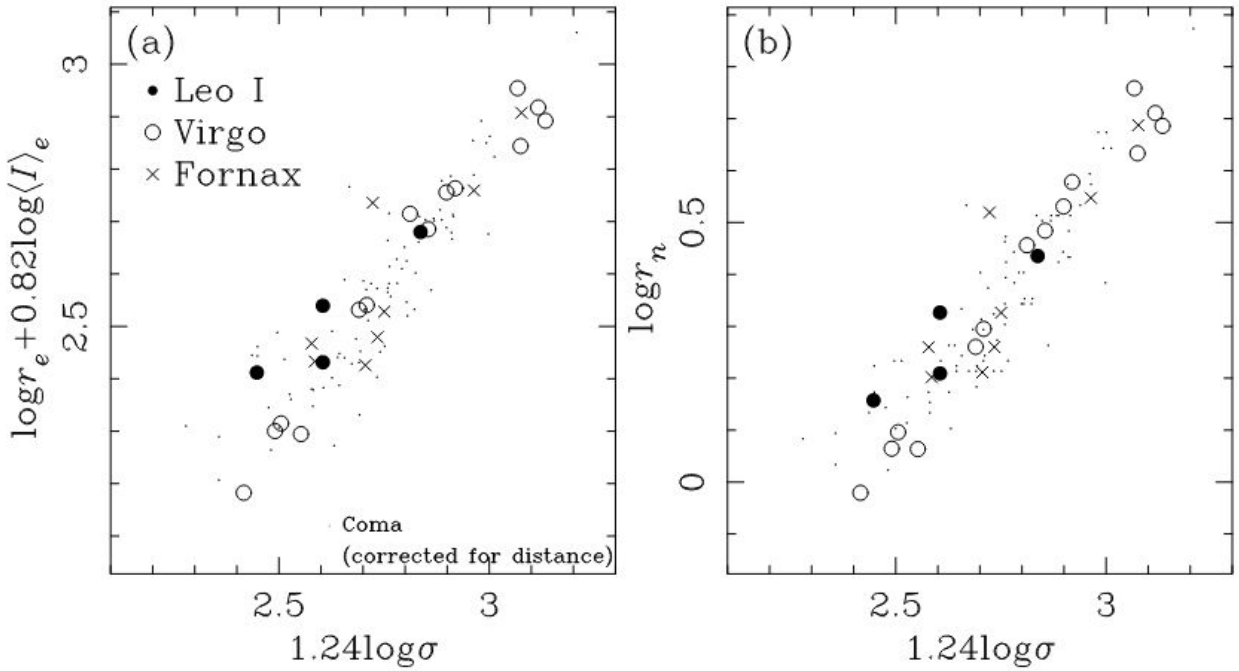

FIG. 2.—(*a*) Fundamental plane and (*b*) D_n-σ relations in Leo I, Virgo, and Fornax, where distance effects have been removed. The Coma sample from Jørgensen et al. (1995a, 1995b) is shown, corrected for distance, by small points.

r_e [kpc] , r_n [kpc]

Kelson et al. 2000, ApJ 529, 768
HST Key Project

- Con la relación de F-J y el plano fundamental se puede determinar distancias de **hasta ~300 Mpc.**

S4- Magnitud absoluta en el máximo de Supernovas tipo Ia (SNIa)

Recordemos que se producen por procesos explosivos de enanas blancas que alcanzan un límite de masa acretada de una compañera, en un sistema binario.

Ventajas: intrínsecamente brillantes, permiten llegar a grandes distancias (**más de 1000 Mpc**, magnitud absoluta en el máximo $M_B \sim -19.5$), y se observan tanto en galaxias E como S.

Son los indicadores secundarios más importantes y proveen la mayor cantidad de trazadores para determinar la constante de Hubble.

However, it turns out that SNe Ia are not really standard candles, since their maximum luminosity varies from object to object with a dispersion of about 0.4 mag in the blue band light.

It turns out that there is a strong correlation between the luminosity and the shape of the light curve of SNe Ia. Those of higher maximum luminosity show a slower decline in the light curve, as measured from its maximum. Furthermore, the observed flux is possibly affected by extinction in the host galaxy, in addition to the extinction in the Milky Way. With the resulting reddening of the spectral distribution, this effect can be derived from the observed colors of the SN. The combined analysis of these effects provides a possibility for deducing an empirical correction to the maximum luminosity from the observed light curves in several filters, accounting both for the relation of the width of the curve to the observed luminosity and for the extinction. This correction was calibrated on a sample of SNe Ia for which the distance to the host galaxies is very accurately known.[9]

Figure **(3)** demonstrates the effect of this correction on the light curves of several SNe Ia which initially appear to have very different maximum luminosities and widths. After correction they become nearly identical. The left panel of Fig. **(3)** suggests that the light curves of SN Ia can basically be described by a one-parameter family of functions, and that this parameter can be deduced from the shape, in particular the width, of the light curves.

With this correction, SNe Ia become standardized candles, i.e., by observing the light curves in several bands their 'corrected' maximum luminosity can be determined. Since the observed flux of a source depends on its luminosity and its distance, once the luminosity is known and the flux measured, the distance to the SN Ia can be inferred

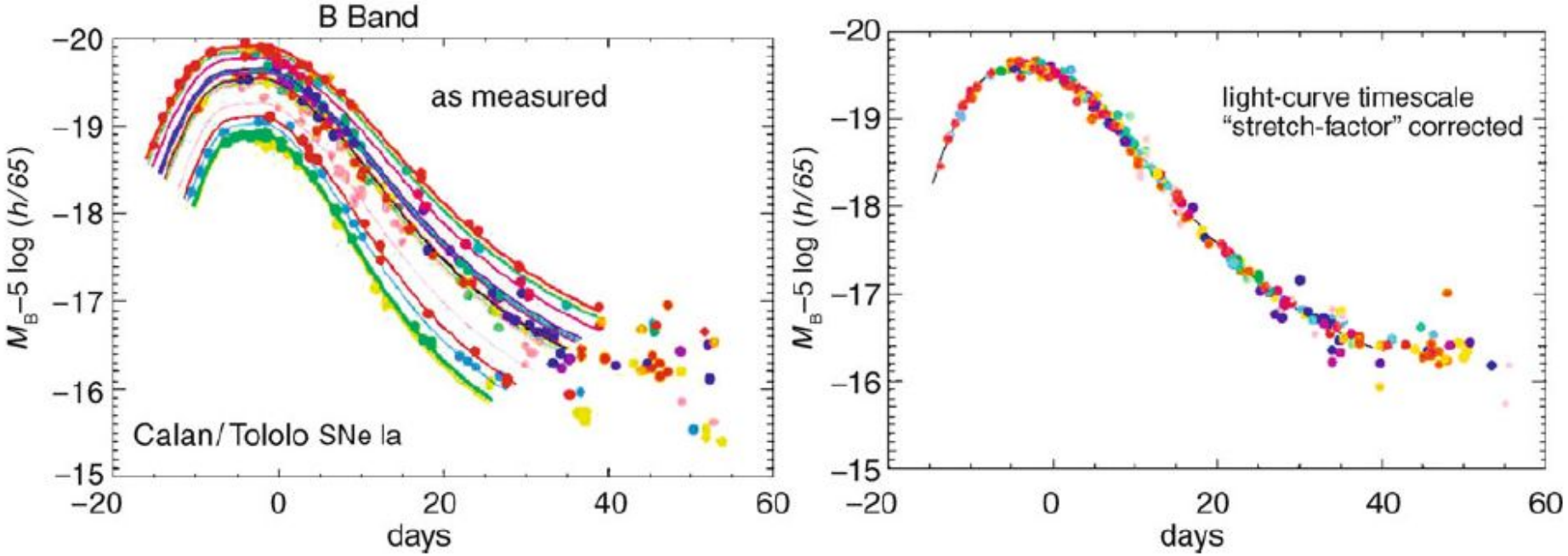

Fig (3) *Left panel*: B-band light curves of different SNe Ia. One sees that the shape of the light curves and the maximum luminosity of the SNe Ia differ substantially among the sample. A transformation was found empirically with a single parameter described by the width of the light curve. By means of this transformation, the different light curves can all be made congruent, as displayed in the *right panel*. Credit: M. Hamuy, S. Perlmutter, Supernova Cosmology Project

Se aplica una *corrección previa* para estandarizar la forma de la curva de luz:
relación entre brillo en el máximo y forma de la curva de luz: más débiles → más empinada

Magnitud absoluta en el máximo de SNIa

TABLE 4

WEIGHTED, METALLICITY-CORRECTED MEAN ABSOLUTE MAGNITUDES OF SNe Ia

Method	M_B	M_V	M_I
1. from μ^0(Gal)	−19.50	−19.47	−19.19
2. from μ_Z^0(LMC)	−19.36	−19.32	−19.07
3. from μ_Z^0(MF)	−19.48	−19.45	−19.20
4. from μ_Z^0 (Paper IV)	−19.49	−19.46	−19.22
Mean of (1)–(4)	−19.46	−19.43	−19.17
Mean of (1), (3), and (4)	−19.49	−19.46	−19.20

NOTE.—The error of the mean is 0.04 mag for all entries.

μ **:** módulo de distancia

Sandage et al. 2006
ApJ 653, 843

❖ **Mag calibradas con la relación P-L de Cefeidas Clásicas:**

1. Cefeidas Galácticas.
2. Cefeidas de la LMC.
3. Cefeidas del artículo de Madore & Freedman (1991, MF)
4. Cefeidas del artículo de Saha et al. (2006, Paper IV)

S5- "Método de fotósferas en expansión" aplicado a Supernovas Tipo II (SNII)

Recordemos que las SNII se producen por el colapso de estrellas masivas (más de 8 masas solares), o sea se originan en poblaciones diferentes que las SNIa. Para determinar distancias se utiliza el *método de fotósferas en expansión (EPM).* Son más débiles que las SNIa y por lo tanto, permiten alcanzar distancias menores (**hasta ~200 Mpc**). Se las detecta más comúnmente en galaxias S, cerca de zonas de formación estelar, por lo que además suelen estar afectadas por extinción interestelar.

***Método EPM*:** It assumes that the expanding shell of hot gases radiates as a blackbody (to a first approximation). Then the supernova's luminosity is given by the Stefan–Boltzmann law,

$$L = 4\pi R^2(t)\sigma T_e^4,$$

where $R(t)$ is the radius of the expanding photosphere and t is the age of the supernova. If we assume that the ejecta's radial velocity has remained nearly constant, then $R(t) = v_{ej}t$. The effective temperature of the photosphere comes from the characteristics of its blackbody spectrum. Once the luminosity is found, it can be converted to an absolute magnitude and then used to find the distance to the supernova by comparing it with the observed apparent magnitude. Of course, the photosphere of the expanding shell of a supernova is neither perfectly spherical nor a perfect blackbody. Difficulties with accurate values for interstellar extinction plague both methods, but the problem is more acute for core-collapse supernovae (Types Ib, Ic, and II), which are found near sites of recent star formation. Typical uncertainties in the distances obtained range from 15% (for M101) to 25% (for the Virgo cluster of galaxies).

Physical Basis of the EPM

EPM is actually a variant of the Baade-Wesselink method, able to produce very accurate results (see Bose and Kumar 2014). The method requires the measurement of the temperature of the expanding stellar envelope, and of the envelope radius, which in turn comes from measurement of time since explosion and the expansion speed from the Doppler shift of the lines. Thus, it allows to measure the absolute luminosity, and finally to obtain the luminosity distance in a direct way. Type II SNe are intrinsicaly bright, so this method is able to provide distance estimates up to cosmological distances, independently from the adopted distance ladder, thus providing an independent check of the results obtained, for example, with the type Ia SNe, and it can be applied at any phase. However, it is observationally demanding, since it requires multi-band photometric data and good quality spectra. Moreover, some modeling is needed, especially in correctly estimating the dilution factor of SNe atmospheric models respect to a pure black body.

S6- Función de luminosidad de Nebulosas Planetarias (FLNP)

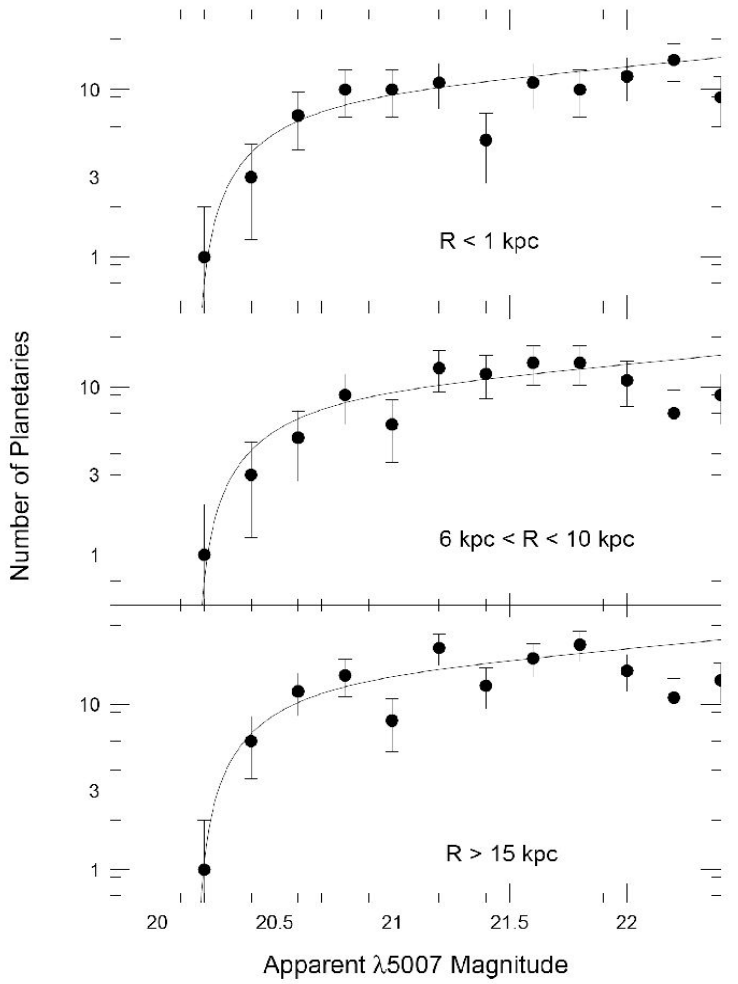

Fig. 6. The observed planetary nebula luminosity functions for samples of M31 PNe projected at three different galactocentric radii. The curves show the best-fitting empirical law. The derived PNLF distances are consisted to within ~0.05 mag. The turnover in the luminosity function past $m_{5007} \gtrsim 22$ in the intermediate and large-radii samples is real, and indicates the presence of relatively massive PN central stars.

Planetary nebulae. The brightness distribution of planetary nebulae in a galaxy seems to have an upper limit which is the nearly the same for each galaxy (see Fig. **6**). If a sufficient number of planetary nebulae are observed and their brightnesses measured, it enables us to determine their luminosity function from which the maximum apparent magnitude is then derived. By calibration on galaxies of known Cepheid distance, the corresponding maximum absolute magnitude can be determined, which then allows the determination of the distance modulus for other galaxies, thus their distances.

Magnitud absoluta del extremo brillante de la FLNP ("cut-off ") es ~constante:

$M(\lambda 5007) \cong -4.5$ mag

Línea de emisión del [OIII] **λ**=5007 Å. Notar que la mag se mide con filtro angosto centrado en esta **λ**.

Ciardullo 2003,
Lecture Notes in Physics 635, 243

Función de luminosidad de Nebulosas Planetarias (FLNP)

Ventajas: las NP son fáciles de identificar, no se requiere mucho tiempo de telescopio, se las encuentra en todo tipo de galaxias, no se ubican en zonas de formación estelar por lo cual no están afectadas por polvo, suele haber cientos de NPs en una galaxia que pueblan el extremo brillante de la FLNP. Su desventaja es que no son intrínsecamente brillantes, por lo permiten alcanzar solo distancias **hasta ~40 Mpc** y con telescopios grandes.

- Cómo se calibra la FLNP, esto es cómo se obtiene la mag de corte "cut-off"?

Con galaxias de distancias determinadas con Cefeidas clásicas (por ej M31, M101, M81, LMC, etc).

- Cómo se aplica?

Se identifican las NP de la galaxia de d desconocida, se construye un histograma de N_o de NP versus mag aparente en 5007Å y se determina cuál es la mag aparente de corte. Conociendo la mag absoluta de corte en la misma λ, se calcula el módulo de distancia.

S7- Función de luminosidad de Cúmulos Globulares (FLCG)

El gráfico de abajo muestra la FLCG de la Vía Láctea: el No de CG asociados a nuestra galaxia en función de sus magnitudes absolutas. Esta FL se puede ajustar con una Gaussiana y lo mismo sucede con los sistemas de CG asociados a otras galaxias, tanto E como S. La particularidad es que el máximo de la Gaussiana (llamado "turn-over") corresponde a una mag absoluta muy similar en prácticamente todos los casos (se diría que es un valor "universal").

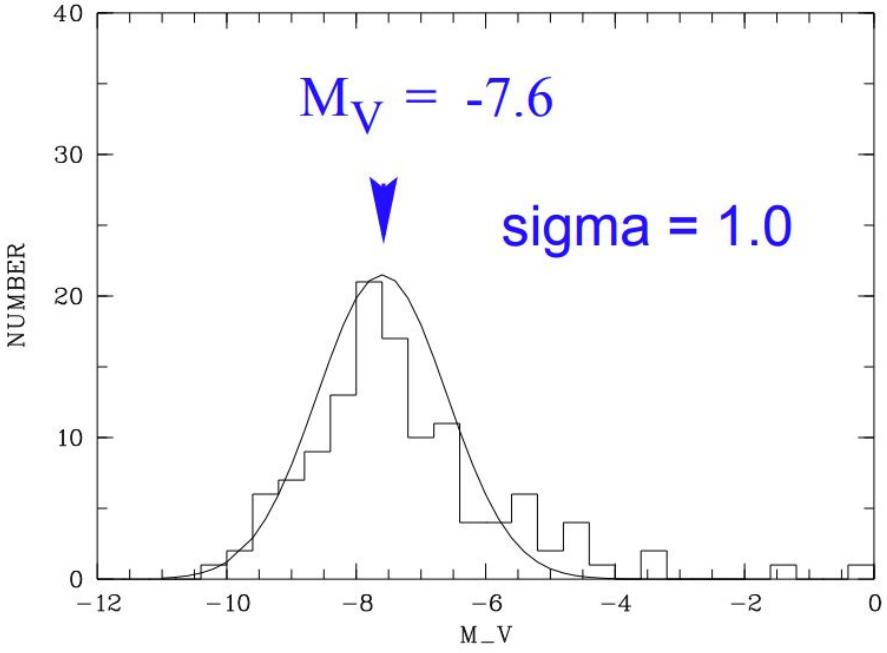

Richtler 2003,
Lecture Notes in Physics 635, 281

Mag absoluta V del máximo de la FLCG:
$M_V \cong$ -7.4 mag

En la Vía Láctea se observa la Gaussiana "completa", en otras galaxias más alejadas no se llegan a detectar los CG más débiles.

La forma Gaussiana se relaciona con la pérdida de CG débiles respecto a los que se formaron originalmente, debido a procesos dinámicos que son más eficientes en destruir los de baja masa.

Función de luminosidad de Cúmulos Globulares (FLCG)

Ventajas: los CG son intrínsecamente brillantes, se pueden observar como objetos puntuales hasta grandes distancias ppalmente en los halos de galaxias y llegar **hasta ~200 Mpc**.

- Cómo se calibra la FLCG, esto es cómo se obtiene la mag del "turn-over"?

Con galaxias de distancias determinadas con Cefeidas clásicas. También en la *Vía Láctea* con *distancias a CG determinadas con RRLyr*.

- Cómo se aplica?

Se identifican los CG de la galaxia de d desconocida, se construye un histograma de N_o de CG vs mag aparente en el filtro observado, se ajusta una Gaussiana y se determina cuál es la mag aparente de su máximo. Conociendo la mag absoluta del máximo en la misma λ, se calcula el módulo de distancia.

La desventaja es que la característica de referencia para determinar distancia (máximo de la Gaussiana) está en la parte más débil de la FL observada para galaxias alejadas, al contrario que la FLNP en que la mag de corte se ubica en la parte brillante de la respectiva FL.

S8- Ley de Hubble- Lemaître / Constante de Hubble H_0

- En octubre de 2018, por votación de sus miembros (78% a favor), la Unión Astronómica Internacional (IAU) recomendó:

Ley de Hubble Ley de Hubble – Lemaître

IAU members vote to recommend renaming the Hubble law as the Hubble - Lemaître law

Ley de Hubble- Lemaître

- Slipher (1914): obtuvo los primeros resultados que indicaban que los espectros de la mayoría de las galaxias estaban “corridos hacia el rojo”.
- Hubble (1929): encontró que esta velocidad estaba relacionada con la distancia.
- Lemaître (1927): *ya había publicado* investigaciones relacionadas con esta relación, pero en una revista de bajo impacto y en francés…

Ese corrimiento al rojo es provocado por la *expansión del Universo, una expansión isotrópica.* Dicha expansión produce el efecto que las galaxias se alejan de nosotros, y cuanto más lejanas, mayor es el corrimiento al rojo (“redshift z”) en sus espectros.

The cosmological redshift

It is possible to characterize the redshift (or blueshift) of a galaxy by the relative difference between the observed and emitted wavelengths of an object. This is given the dimensionless quantity, z. From the definitions of z it is then possible to derive the alternate forms shown below:

$$z = \frac{\lambda_{observed} - \lambda_{emitted}}{\lambda_{emitted}}$$

$$1 + z = \frac{\lambda_{observed}}{\lambda_{emitted}}$$

$$c\,z = H_0\,d$$

cte de Hubble H_0 $\left[\frac{km}{s\,Mpc}\right]$

distancia d [Mpc]

válido para z<< 1
(caso no relativista)

“Redshift” *no* es lo mismo que un corrimiento Doppler:

Morison, I: “Introduction to Astronomy and Cosmology”

In the above, the blueshift and redshift were regarded as being due to the Doppler effect, and this would be perfectly correct when considering the blue shifts shown by the galaxies in the Local Group. However, in the cases of galaxies beyond our Local Group there is a far better way of thinking about the cause of the redshifts that are observed by us. It is not right to think of the galaxies (beyond the movements of those in our Local Group) moving through space but, rather, that they are being carried apart by the expansion of space. A nice analogy is that of baking a currant bun. The dough is packed with currants and then baked. When taken out of the oven the bun will (hopefully) be bigger and thus the currants will be further apart. They will not have moved *through* the dough, but will have been carried apart by the *expansion* of the dough.

As Hubble showed, the universe is expanding so that it would have been smaller in the past. When a photon was emitted in a distant galaxy corresponding to a specific spectral line, the universe would have been smaller. In the time it has taken that photon to reach us whilst the photon has travelled through space, the universe has expanded and this expansion has stretched, by exactly the same ratio, the wavelength of the photon. This increases the wavelength so giving rise to a redshift that we call the ‘cosmological redshift’. A simple analogy is that of drawing a sine wave (representing the wavelength of a photon) onto a slightly blown up balloon. If the balloon is then blown up further, the length between the peaks of the sine wave (its wavelength) will increase.

Constante de Hubble H_0

Hubble constant = rate of expansion in units of (km/s)/Mpc

✔ Resultado del *Key Project del HST*: $H_0 = 72 \pm 8$ km / s Mpc
(Freedman et al. 2001, ApJ 553, 47)

✔ Sandage, Tammann et al. 2006, $H_0 = 62.3 \pm 6.3$ km / s Mpc
ApJ 653, 843

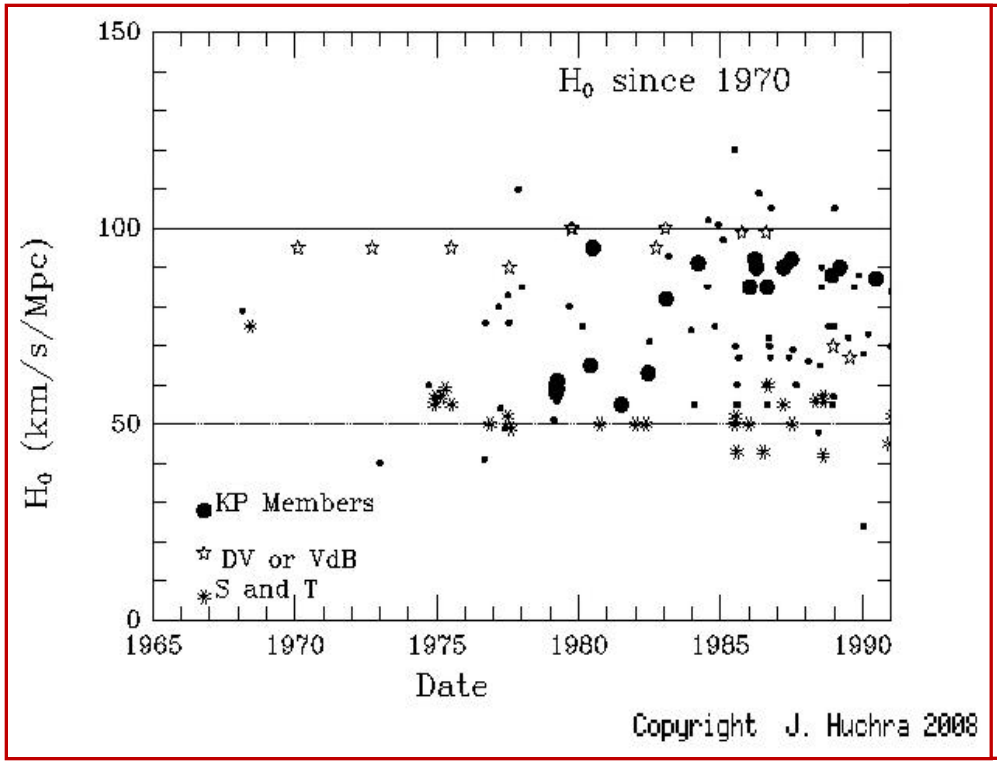

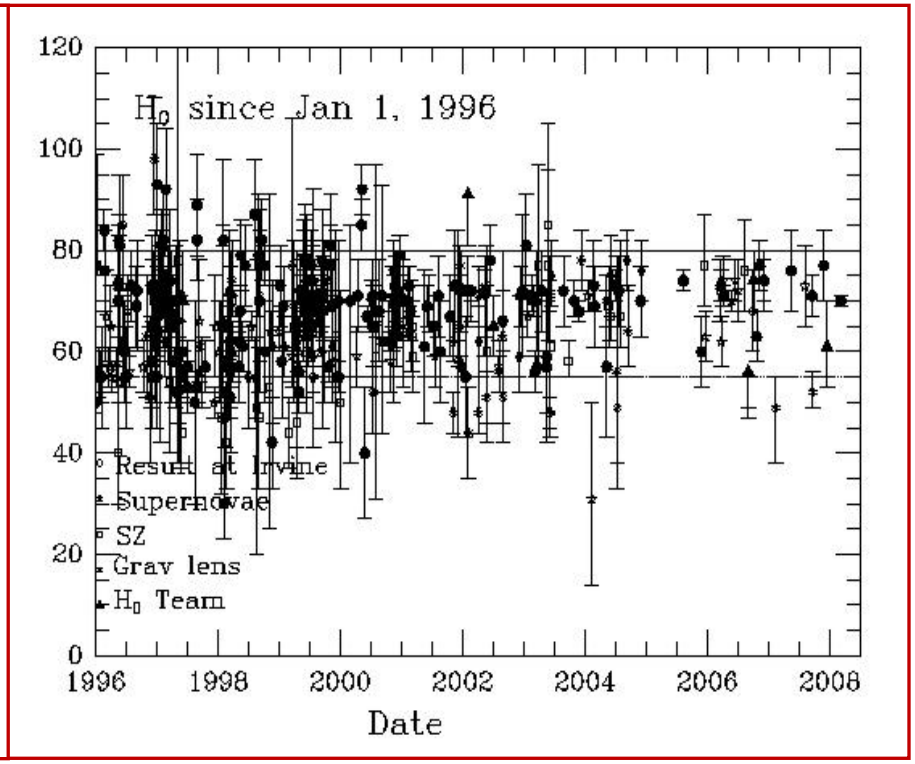

Constante de Hubble H_0

✔ Riess et al. 2011, ApJ 730, 119 H_0 = 73.8 ± 2.4 km / s Mpc (error 3.3%)

(ver siguiente slide)

✔ Riess et al. 2018, ApJ 861, #126 H_0 = 73.52 ± 1.62 km / s Mpc (error 2.2%)

(50 Cef. de la Vía Láctea, fotometría HST + paralajes Gaia DR2)

✔ Riess et al. 2019, ApJ 876, #85 **H_0 = 74.03 ± 1.42 km / s Mpc (error 1.9%)**

(70 Cef. de la LMC, fotometría HST + d LMC (bin. eclip. + SNIa))

Cefeidas en la galaxia NGC 5584 (d = 24 Mpc, SNIa en 2007)

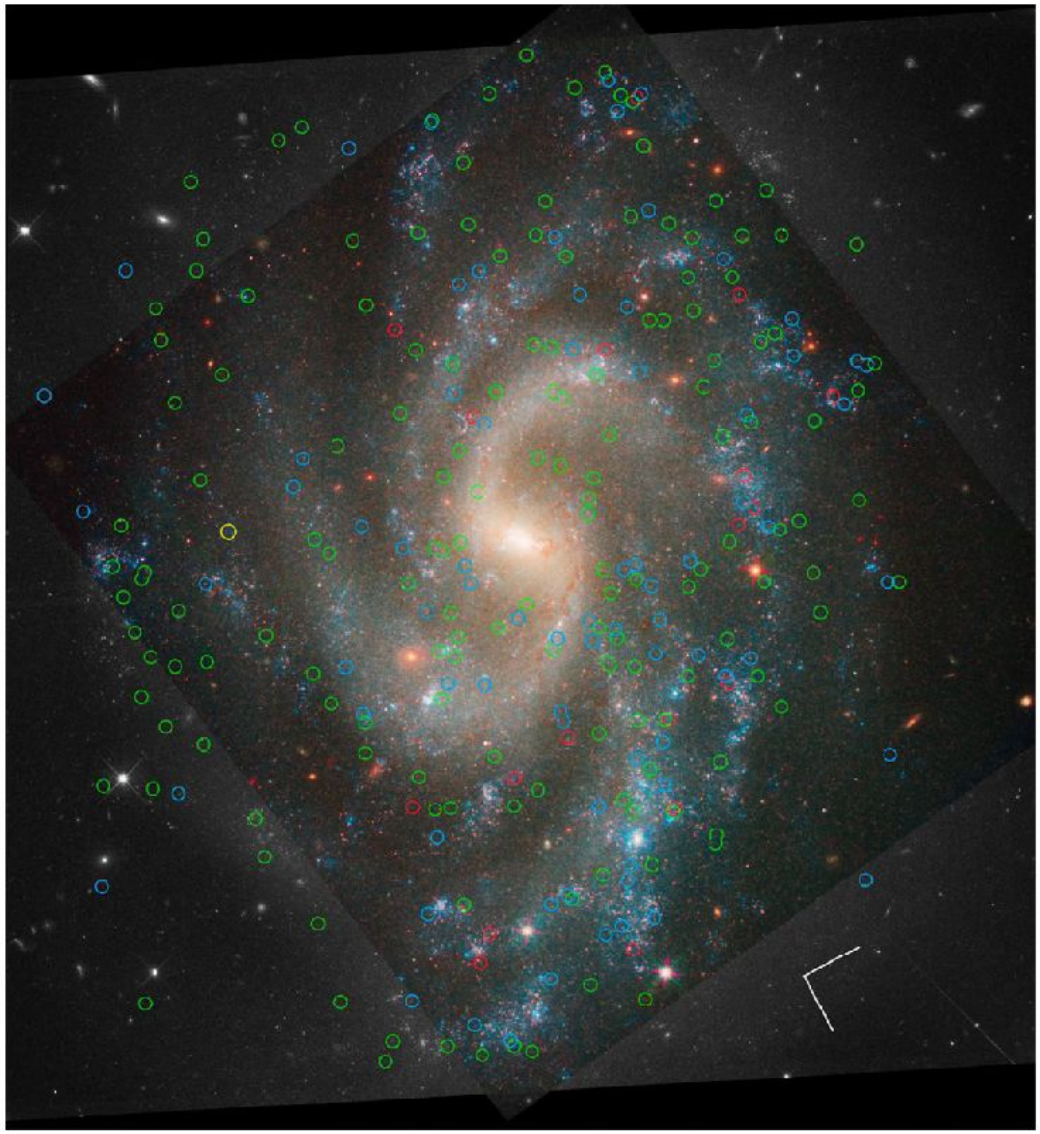

Figure 2. *HST* images of NGC 5584. The positions of Cepheids with periods in the range $P > 60$ days, 30 days $< P < 60$ days, and 10 days $< P < 30$ days are indicated by red, blue, and green circles, respectively. A yellow circle indicates the position of the host galaxy's SN Ia. The orientation is indicated by the compass rose whose vectors have lengths of 15″ and indicate north and east. The black and white regions of the images show the WFC3 optical data and the color includes the WFC3–IR data.

Riess et al. (2011)

Constante de Hubble H_0

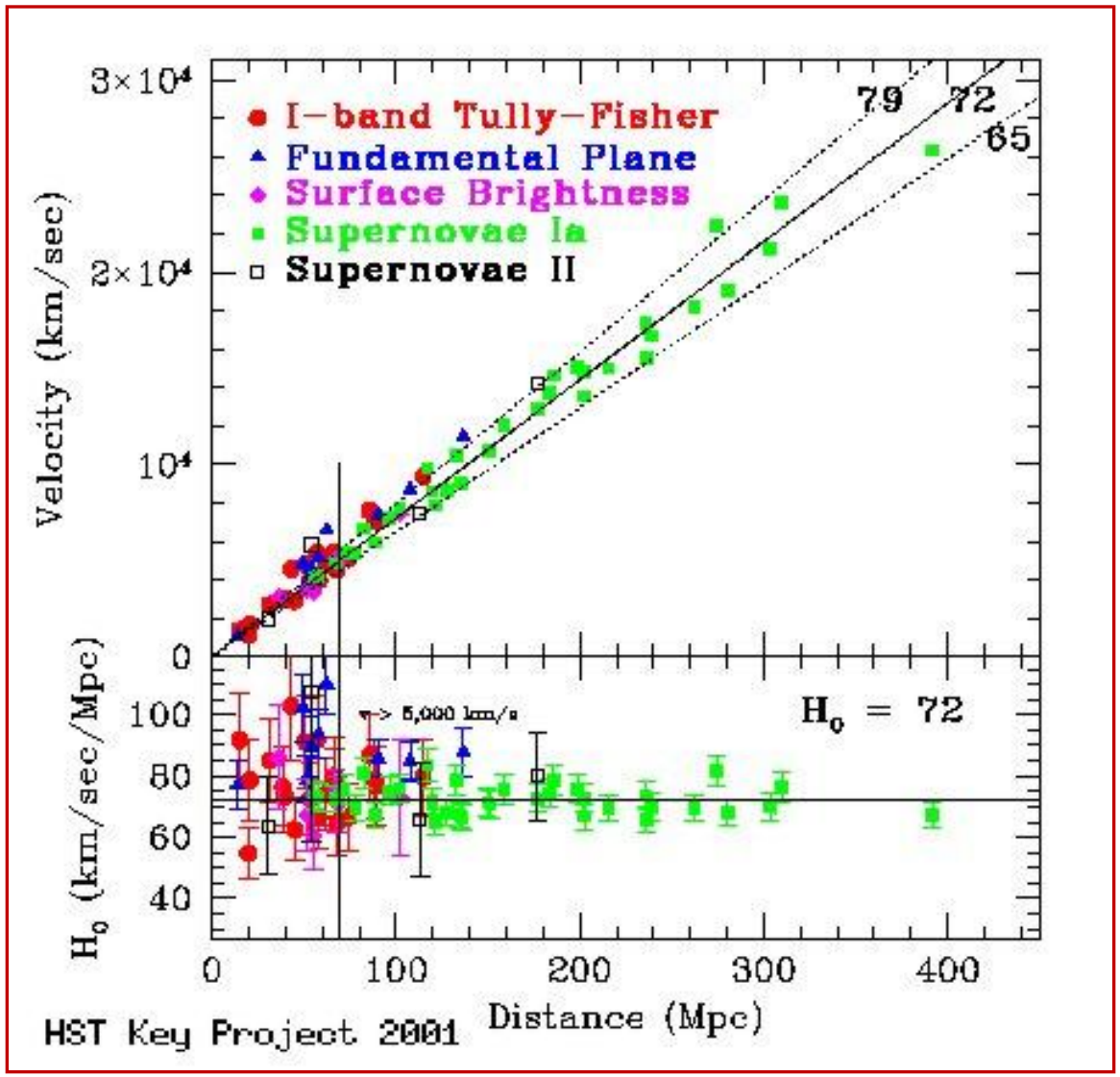

Velocidades peculiares:

Carroll & Ostlie: "An Introduction to Modern Astrophysics"

There is a vital distinction between the velocity of a galaxy through space (called its **peculiar velocity**) and its **recessional velocity** due to the expansion of the universe. A galaxy's recessional velocity is *not* due to its motion through space; instead, the galaxy is being carried along *with* the surrounding space as the universe expands. The motion of galaxies as they participate in the expansion of the universe is referred to as the **Hubble flow**. In the same manner, a galaxy's **cosmological redshift** is produced by the expansion as the wavelength of the light emitted by the galaxy is stretched along with the space through which the light travels. For this reason, the cosmological redshift is not related to the galaxy's recessional velocity by the Doppler shift equations.

Nevertheless, astronomers frequently translate a measured redshift, z, into the radial velocity a galaxy would have, *as if* it had a peculiar velocity (moving through space) instead of its actual recessional velocity (moving along with expanding space).

- Las *velocidades peculiares* son consecuencia de la atracción gravitatoria entre galaxias y objetos de mayor masa (grupos, cúmulos, filamentos, etc). Pueden ser positivas o negativas.

La velocidad radial que se mide incluye dos componentes (donde V_{pec} es la veloc pec en la dirección radial):

$$V_{rad} = V_{recesion} + V_{pec} = H_0\, d + V_{pec}$$

Típicamente las V_{pec} son del orden de algunos cientos de km/s sobre escalas del orden de decenas de Mpc. Por lo tanto, se trata de medir H_0 sobre escalas mayores, para que $V_{recesion} >> V_{pec}$, que corresponde al régimen del *flujo de Hubble*.

Another Problem: Peculiar Velocities

- Note that we can in practice only observe the radial component
- Peculiar velocities act as a noise (on the $V = cz$ axis, orthogonal to errors in distances) in the Hubble diagram - and could thus bias the measurements of the H_0 (which is why we want "far field" measurements)

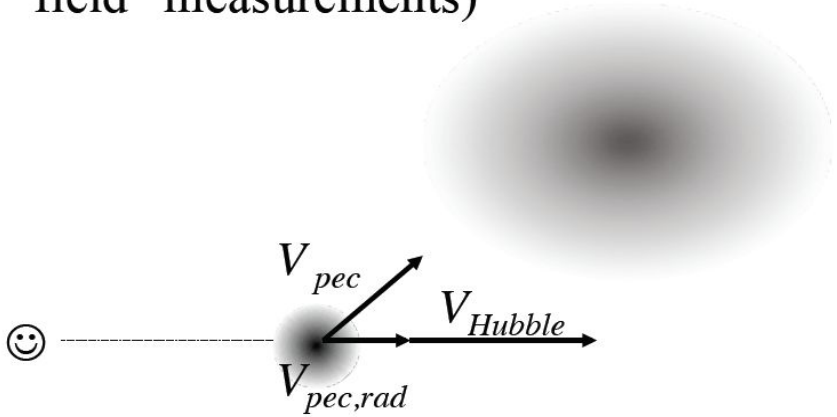

$$V_{total} = V_{Hubble} + V_{pec,rad}$$

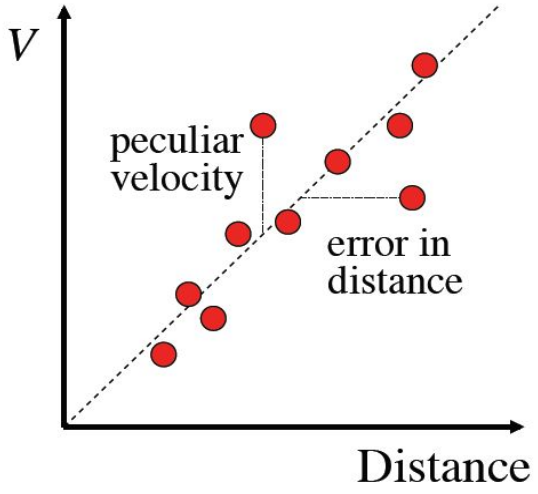

S. Djorgovski, 2013

La velocidad peculiar del Grupo Local respecto al flujo de Hubble se calcula en ~630 km/s. Parte de ese movimiento se debe a la atracción del cúmulo de Virgo (el llamado “Virgocentric infall”) que se estima en ~170 km/s, esto es un 27% de la Vpec.

$$h = H_0 \,/100 \left[\frac{\text{km}}{\text{s Mpc}}\right]$$

The Virgocentric peculiar velocity is a minor perturbation in a much larger scale inhomogeneity in the Hubble flow. There is a large-scale streaming motion (relative to the Hubble flow) that carries the Milky Way, the Local Group, the Virgo cluster, and thousands of other galaxies through space in the direction of the constellation Centaurus. The peculiar velocity of the Local Group relative to the Hubble flow is 627 km s^{-1}. This riverlike motion of thousands of galaxies extends at least $40h^{-1}$ Mpc both upstream and downstream. Astronomers would like to use this streaming to deduce the location(s) of the mass, visible or dark, capable of exerting such an immense gravitational tug. The Hydra–Centaurus supercluster, which is in the direction of the flow, is *not* responsible, since it too is moving along with the flow of the rest of the galaxies. This implies that the source of the motion lies beyond that supercluster.

In the 1980s, American astronomers Alan Dressler and Sandra Faber calculated the presence of a **Great Attractor** (GA), a diffuse collection of clusters spread over a wide (60°) region of the sky. According to their calculations, the GA lies in the same plane as the Local Supercluster, about $42h^{-1}$ Mpc away in the direction of $\ell = 309°$, $b = 18°$ (Galactic coordinates) in the constellation Centaurus. The mass of the Great Attractor is estimated to be about $2 \times 10^{16} h^{-1}$ $M_\odot$, but there are just 7,500 galaxies known in that region—too few to account for so much mass. This suggests that approximately 90% of the mass of the GA may be in the form of dark matter.

Another possibility is that the Great Attractor is not solely responsible for the large-scale streaming motion. The **Shapley concentration** of galaxies is probably the most massive collection of galaxies in our neighborhood of the universe. With a core consisting of a gravitationally bound concentration of some 20 rich clusters of galaxies, the Shapley concentration has a mass of a few $\times 10^{16} h^{-1}$ $M_\odot$ and lies within 10° of the direction of the Local Group's motion and very close to the direction of the Great Attractor. However, its distance of $140h^{-1}$ Mpc is three times the distance calculated for the Great Attractor, so it cannot be identified with the GA. Still, it is probably responsible for 10–15% of the net acceleration of the Local Group.

Carroll & Ostlie: "An Introduction to Modern Astrophysics"

If the distance to each galaxy from Earth is directly measured, then the peculiar velocity can be derived from the subtraction of the mean cosmic expansion, the product of distance times the Hubble constant, from observed velocity. The peculiar velocity is the line-of-sight departure from the cosmic expansion and arises from gravitational perturbations; a map of peculiar velocities can be translated into a map of the distribution of matter[3]. Here we report a map of structure made using a catalogue of peculiar velocities. We find locations where peculiar velocity flows diverge, as water does at watershed divides, and we trace the surface of divergent points that surrounds us. Within the volume enclosed by this surface, the motions of galaxies are inward after removal of the mean cosmic expansion and long range flows. We define a supercluster to be the volume within such a surface, and so we are defining the extent of our home supercluster, which we call Laniakea.

Tully et al. 2014, Nature 513, 71

El supercúmulo de Shapley

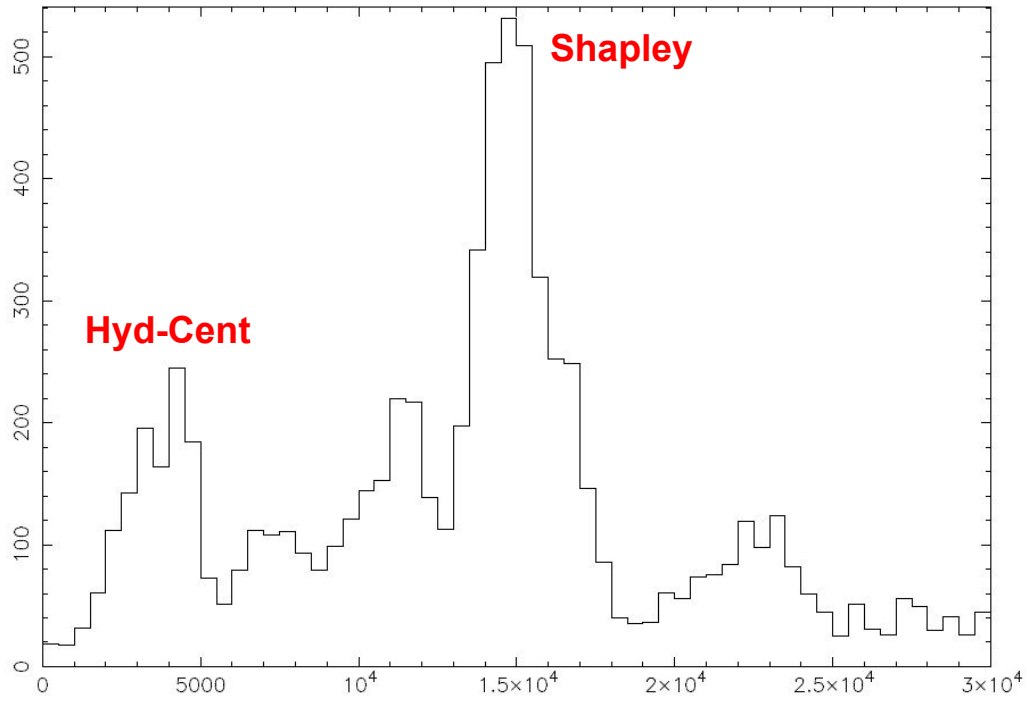

Fig. 2. Histogram of galaxy velocities in the direction of the Shapley Supercluster with all velocities available in the range 0 $\mathrm{km\,s^{-1}} \leq v \leq 30000$ $\mathrm{km\,s^{-1}}$, with a step size of 500 $\mathrm{km\,s^{-1}}$.

Proust et al. 2006,
A&A 447, 133

El supercúmulo Laniakea

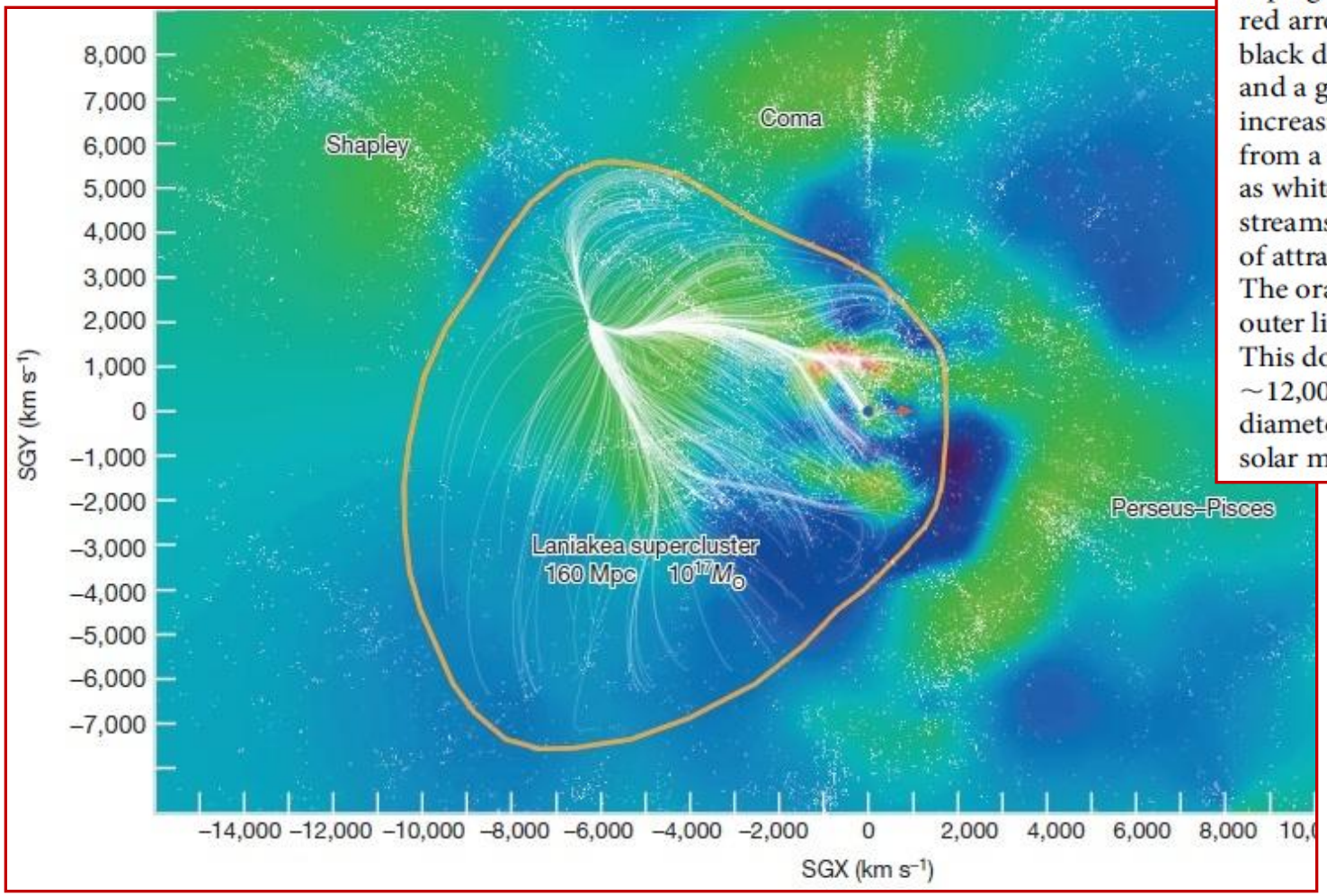

Figure 2 | A slice of the Laniakea supercluster in the supergalactic equatorial plane. Shaded contours represent density values within the equatorial slice, with red at high densities, green at intermediate densities and blue in voids. Our Milky Way galaxy is located at the black dot at the origin of the supergalactic coordinates system: a red arrow points right from the black dot toward increasing SGX and a green arrow points up toward increasing SGY. Individual galaxies from a redshift catalogue are given as white dots. Velocity flow streams within the Laniakea basin of attraction are shown in white. The orange contour encloses the outer limits of these streams. This domain has a extent of $\sim$12,000 km s^{-1} ($\sim$160 Mpc diameter) and encloses $\sim 10^{17}$ solar masses, $M_\odot$.

Tully et al. 2014

Escala de distancias completa "aproximada"

Geometry:

- MW: 15 trig. parallaxes of Cepheids

- LMC and M31: detached eclipsing binaries

- NGC 4258: water masers

Riess et al. 2016, ApJ 826, 56

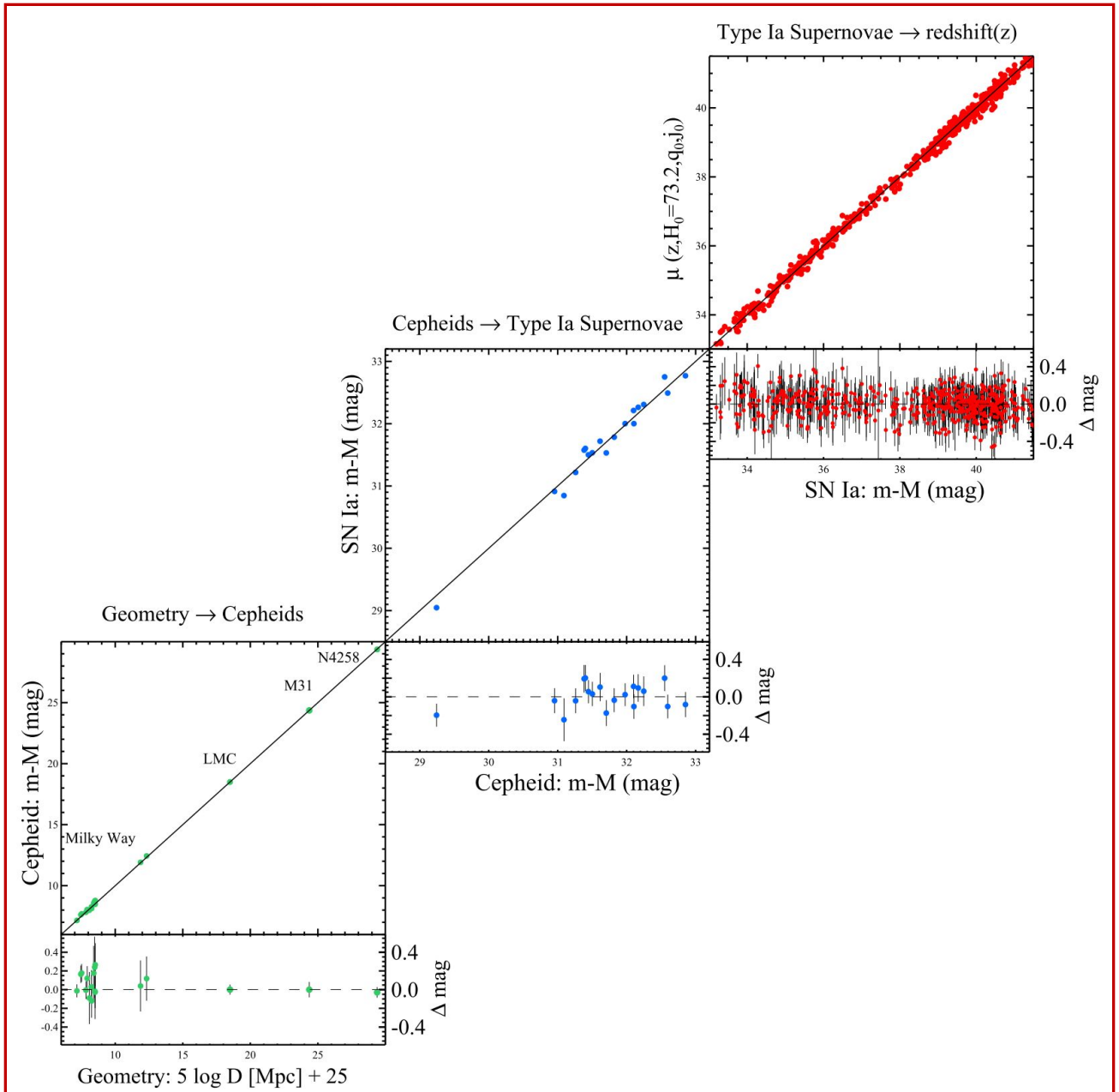

Figure 10. Complete distance ladder. The simultaneous agreement of pairs of geometric and Cepheid-based distances (lower left), Cepheid and SN Ia-based distances (middle panel) and SN and redshift-based distances provides the measurement of the Hubble constant. For each step, geometric or calibrated distances on the *x*-axis serve to calibrate a relative distance indicator on the *y*-axis through the determination of M or H_0. Results shown are an approximation to the global fit as discussed in the text.